

Fundamental limits on the rate of bacterial cell division

Nathan M. Belliveau^{†, 1}, Griffin Chure^{†, 2, 3}, Christina L. Hueschen⁴, Hernan G. Garcia⁵, Jané Kondev⁶, Daniel S. Fisher⁷, Julie Theriot^{1, 8}, Rob Phillips^{2, 9,*}

*For correspondence:

[†]These authors contributed equally to this work

¹Department of Biology, University of Washington, Seattle, WA, USA; ²Division of Biology and Biological Engineering, California Institute of Technology, Pasadena, CA, USA; ³Department of Applied Physics, California Institute of Technology, Pasadena, CA, USA; ⁴Department of Chemical Engineering, Stanford University, Stanford, CA, USA; ⁵Department of Molecular Cell Biology and Department of Physics, University of California Berkeley, Berkeley, CA, USA; ⁶Department of Physics, Brandeis University, Waltham, MA, USA; ⁷Department of Applied Physics, Stanford University, Stanford, CA, USA; ⁸Allen Institute for Cell Science, Seattle, WA, USA; ⁹Department of Physics, California Institute of Technology, Pasadena, CA, USA; *Contributed equally

Abstract This will be written next

Introduction

The range of bacterial growth rates is enormously diverse. In natural environments, some microbial organisms might double only once per year while in comfortable laboratory conditions, growth can be rapid with several divisions per hour. This six order of magnitude difference illustrates the intimate relationship between environmental conditions and the rates at which cells convert nutrients into new cellular material – a relationship that has remained a major topic of inquiry in bacterial physiology for over a century (*Jun et al., 2018*). As was noted by Jacques Monod, “the study of the growth of bacterial cultures does not constitute a specialized subject or branch of research, it is the basic method of Microbiology.” Those words ring as true today as they did when they were written 70 years ago. Indeed, the study of bacterial growth has undergone a molecular resurgence since many of the key questions addressed by the pioneering efforts in the middle of the last century can be revisited by examining them through the lens of the increasingly refined molecular census that is available for bacteria such as the microbial workhorse *Escherichia coli*. Several of the outstanding questions that can now be studied about bacterial growth include: what sets the fastest time scale that bacteria can divide, and how is growth rate tied to the quality of the carbon source. In this paper, we address these two questions from two distinct angles. First, as a result of an array of high-quality proteome-wide measurements of the *E. coli* proteome under a myriad of different growth conditions, we have a census that allows us to explore how the number of key molecular players change as a function of growth rate. This census provides a window onto whether the processes they mediate such as molecular transport into the cells and molecular synthesis within cells can run faster. Second, because of our understanding of the molecular pathways responsible for many of the steps in bacterial growth, we can also make order of magnitude estimates to infer the copy numbers that would be needed to achieve a given growth rate. In this paper, we pass back and forth between the analysis of a variety of different proteomic datasets and order-of-magnitude estimations to determine possible molecular bottlenecks that limit bacterial growth and to see how

42 the growth rate varies in different carbon sources.

43 Specifically, we leverage a combination of *E. coli* proteomic data sets collected over the past
 44 decade using either mass spectrometry (*Schmidt et al., 2016; Peebo et al., 2015; Valgepea et al.,*
 45 **2013**) or ribosomal profiling (*Li et al., 2014*) across 31 unique growth conditions. Broadly speaking,
 46 we entertain several classes of hypotheses as are illustrated in **Figure 1**. First, we consider potential
 47 limits on the transport of nutrients into the cell. We address this hypothesis by performing an
 48 order-of-magnitude estimate for how many carbon, phosphorous, and sulfur atoms are needed to
 49 facilitate this requirement given a 5000 second division time. As a second hypothesis, we consider
 50 the possibility that there exists a fundamental limit on how quickly the cell can generate ATP. We
 51 approach this hypothesis from two angles, considering how many ATP synthase complexes must
 52 be needed to churn out enough ATP to power protein translation followed by an estimation of
 53 how many electron transport complexes must be present to maintain the proton motive force.
 54 A third class of estimates considers the need to maintain the size and shape of the cell through
 55 the construction of new lipids for the cell membranes as well as the glycan polymers which make
 56 up the rigid peptidoglycan. Our final class of hypotheses centers on the synthesis of a variety of
 57 biomolecules. Our focus is primarily on the stages of the central dogma as we estimate the number
 58 of protein complexes needed for DNA replication, transcription, and protein translation.

59 In broad terms, we find that the majority of these estimates are in close agreement with the
 60 experimental observations, with protein copy numbers apparently well-tuned for the task of cell
 61 doubling. This allows us to systematically scratch off the hypotheses diagrammed in **Figure 1** as
 62 setting possible speed limits. Ultimately, we find that protein translation (particularly the generation
 63 of new ribosomes) acts as 1) a rate limiting step for the *fastest* bacterial division, and 2) the major
 64 determinant of bacterial growth across all nutrient conditions we have considered under steady
 65 state, exponential growth. This perspective is in line with the linear correlation observed between
 66 growth rate and ribosomal content (typically quantified through the ratio of RNA to protein) for fast
 67 growing cells (*Scott et al., 2010*), but suggests a more prominent role for ribosomes in setting the
 68 doubling time across all conditions of nutrient limitation. Here we again leverage the quantitative
 69 nature of this data set and present a quantitative model of the relationship between the fraction of
 70 the proteome devoted to ribosomes and the speed limit of translation, revealing a fundamental
 71 tradeoff between the translation capacity of the ribosome pool and the maximal growth rate.

72 Uptake of Nutrients

73 In order to build new cellular mass, the molecular and elemental building blocks must be scavenged
 74 from the environment in different forms. Carbon, for example, is acquired via the transport of
 75 carbohydrates and sugar alcohols with some carbon sources receiving preferential treatment
 76 in their consumption (*Monod, 1947*). Phosphorus, sulfur, and nitrogen, on the other hand, are
 77 harvested primarily in the forms of inorganic salts, namely phosphate, sulfate, and ammonia
 78 (*Jun et al., 2018; Assentoft et al., 2016; Stasi et al., 2019; Antonenko et al., 1997; Rosenberg et al.,*
 79 **1977; Willsky et al., 1973**). All of these compounds have different permeabilities across the cell
 80 membrane *Phillips (2018)* and most require some energetic investment either via ATP hydrolysis
 81 or through the proton electrochemical gradient to bring the material across the hydrophobic cell
 82 membrane. Given the diversity of biological transport mechanisms and the vast number of inputs
 83 needed to build a cell, we begin by considering transport of some of the most important cellular
 84 ingredients: carbon, nitrogen, oxygen, hydrogen, phosphorus, and sulfur.

85 The elemental composition of *E. coli* has received much quantitative attention over the past
 86 half century (*Neidhardt et al., 1991; Taymaz-Nikerel et al., 2010; Heldal et al., 1985; Bauer and Ziv,*
 87 **1976**), providing us with a starting point for estimating the copy numbers of various transporters.
 88 While there is some variability in the exact elemental percentages (with different uncertainties), we
 89 can estimate that the dry mass of a typical *E. coli* cell is \approx 45% carbon (BNID: 100649, *Milo et al.*
 90 **(2010)**), \approx 15% nitrogen (BNID: 106666, *Milo et al. (2010)*), \approx 3% phosphorus (BNID: 100653, *Milo*
 91 *et al. (2010)*), and 1% sulfur (BNID: 100655, *Milo et al. (2010)*). In the coming paragraphs, we will

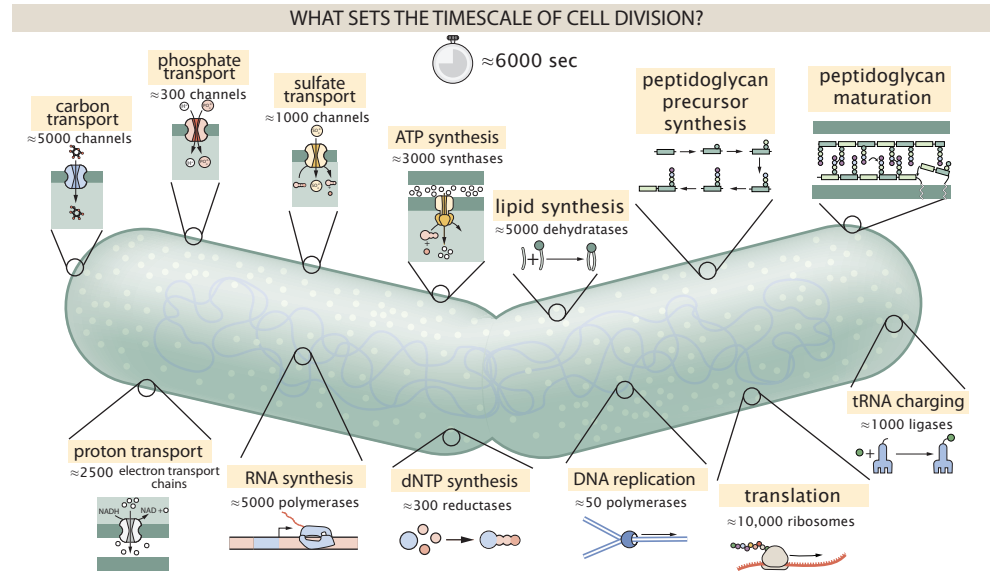


Figure 1. Transport and synthesis processes necessary for cell division. We consider an array of processes necessary for a cell to double its molecular components. Such processes include the transport of carbon across the cell membrane, the production of ATP, and fundamental processes of the central dogma namely RNA, DNA, and protein synthesis. A schematic of each synthetic or transport category is shown with an approximate measure of the complex abundance at a growth rate of 0.5 per hour. In this work, we consider a standard bacterial division time of ≈ 5000 sec.

engage in a dialogue between back-of-the-envelope estimates for the numbers of transporters needed to facilitate these chemical stoichiometries and the experimental proteomic measurements of the biological reality. Such an approach provides the opportunity to test if our biological knowledge is sufficient to understand the scale at which these complexes are produced. Specifically, we will make these estimates considering a modest doubling time of 5000 s, a growth rate of $\approx 0.5 \text{ hr}^{-1}$, the range in which the majority of the experimental measurements reside.

Nitrogen Transport

Before we begin our back-of-the-envelope estimations, we must address which elemental sources must require proteinaceous transport, meaning that the cell cannot acquire appreciable amounts simply via diffusion from the membrane. The permeability of the lipid membrane to a large number of solutes has been extensively characterized over the past century. Large, polar molecular species (such as various sugar molecules, sulfate, and phosphate) have low permeabilities while small, non-polar compounds (such as oxygen, carbon dioxide, and ammonia) can readily diffuse across the membrane. Ammonia, a primary source of nitrogen in typical laboratory conditions, has a permeability on par with water ($\approx 10^5 \text{ nm/s}$, BNID:110824 *Milo et al. (2010)*). In particularly nitrogen-poor conditions, *E. coli* expresses a transporter (AmtB) which appears to aid in nitrogen assimilation, though the mechanism and kinetic details of transport is still a matter of debate (*van Heeswijk et al., 2013; Khademi et al., 2004*). Beyond ammonia, another plentiful source of nitrogen come in the form of glutamate, which has its own complex metabolism and scavenging pathways. However, nitrogen is plentiful in the growth conditions examined in this work, permitting us to neglect nitrogen transport as a potential rate limiting process in cell division in typical experimental conditions. We direct the reader to the supplemental information for a more in-depth discussion of permeabilities and a series of calculations revealing that active nitrogen transport can be neglected for the purposes of this article.

116 **Carbon Transport**

117 We begin our estimations with the most abundant element in *E. coli* by mass, carbon. Using
 118 ≈ 0.3 pg as the typical *E. coli* dry mass (BNID: 103904, *Milo et al. (2010)*), we estimate that \approx
 119 10^{10} carbon atoms must be brought into the cell in order to double all of the carbon-containing
 120 molecules (*Figure 2(A, top)*). Typical laboratory growth conditions, such as those explored in the
 121 aforementioned proteomic data sets, provide carbon as a single class of sugar such as glucose,
 122 galactose, or xylose to name a few. *E. coli* has evolved myriad mechanisms by which these sugars can
 123 be transported across the cell membrane. One such mechanism of transport is via the PTS system
 124 which is a highly modular system capable of transporting a diverse range of sugars (*Escalante et al., 2012*).
 125 The glucose-specific component of this system transports ≈ 200 glucose molecules per second per transporter (BNID: 114686, *Milo et al. (2010)*). Making the assumption that this is a
 126 typical sugar transport rate, coupled with the need to transport 10^{10} carbon atoms, we arrive at the
 127 conclusion that on the order of 1,000 transporters must be expressed in order to bring in enough
 128 carbon atoms to divide in 5000 s, diagrammed in the top panel of *Figure 2(A)*. This estimate, along
 129 with the observed average number of the PTS system carbohydrate transporters present in the
 130 proteomic data sets (*Schmidt et al., 2016; Peebo et al., 2015; Valgepea et al., 2013; Li et al., 2014*),
 131 is shown in *Figure 2(A)*. While we estimate 1500 transporters are needed with a 5000 s division
 132 time, we can abstract this calculation to consider any particular growth rate given knowledge of
 133 the cell density and volume as a function of growth rate and direct the reader to the SI for more
 134 information. As revealed in *Figure 2(A)*, experimental measurements exceed the estimate by several
 135 fold, illustrating that transport of carbon in to the cell is not rate limiting for cell division. Abstracting
 136 this point estimate at 5000 s to a continuum of growth rates (grey line in *Figure 2(A)*) reveals an
 137 excess of transporters at other growth rates, though in rapid growth regimes, the abundance is
 138 below our simple estimate.
 139

140 The estimate presented in *Figure 2(A)* neglects any specifics of the regulation of carbon transport
 141 system and presents a data-averaged view of how many carbohydrate transporters are present
 142 on average. Using the diverse array of growth conditions explored in the proteomic data sets, we
 143 can explore how individual carbon transport systems depend on the population growth rate. In
 144 *Figure 2(B)*, we show the total number of carbohydrate transporters specific to different carbon
 145 sources. A striking observation, shown in the top-left plot of *Figure 2(B)*, is the constancy in the
 146 expression of the glucose-specific transport systems. Additionally, we note that the total number
 147 of glucose-specific transporters is tightly distributed $\approx 10^4$ per cell, the approximate number of
 148 transporters needed to sustain rapid growth of several divisions per hour. This illustrates that *E. coli*
 149 maintains a substantial number of complexes present for transporting glucose which is known
 150 to be the preferential carbon source (*Monod, 1947; Liu et al., 2005; Aidelberg et al., 2014*).

151 It is now understood that a large number of metabolic operons are regulated with dual-input
 152 logic gates that are only expressed when glucose concentrations are low (mediated by cyclic-AMP
 153 receptor protein CRP) and the concentration of other carbon sources are elevated (*Gama-Castro et al., 2016; Zhang et al., 2014b*). A famed example of such dual-input regulatory logic is in the
 154 regulation of the *lac* operon which is only natively activated in the absence of glucose and the
 155 presence of allolactose, an intermediate in lactose metabolism (*Jacob and Monod, 1961*), though we
 156 now know of many other such examples (*Ireland et al., 2020; Gama-Castro et al., 2016; Belliveau et al., 2018*). This illustrates that once glucose is depleted from the environment, cells have a means
 157 to dramatically increase the abundance of the specific transporter needed to digest the next sugar
 158 that is present. Several examples of induced expression of specific carbon-source transporters
 159 are shown in *Figure 2(B)*. Points colored in red (labeled by red text-boxes) correspond to growth
 160 conditions in which the specific carbon source (glycerol, xylose, or fructose) is present. These
 161 plots show that, in the absence of the particular carbon source, expression of the transporters
 162 is maintained on the order of $\sim 10^2$ per cell. However, when the transport substrate is present,
 163 expression is induced and the transporters become highly-expressed. The grey lines in *Figure 2(B)*
 164

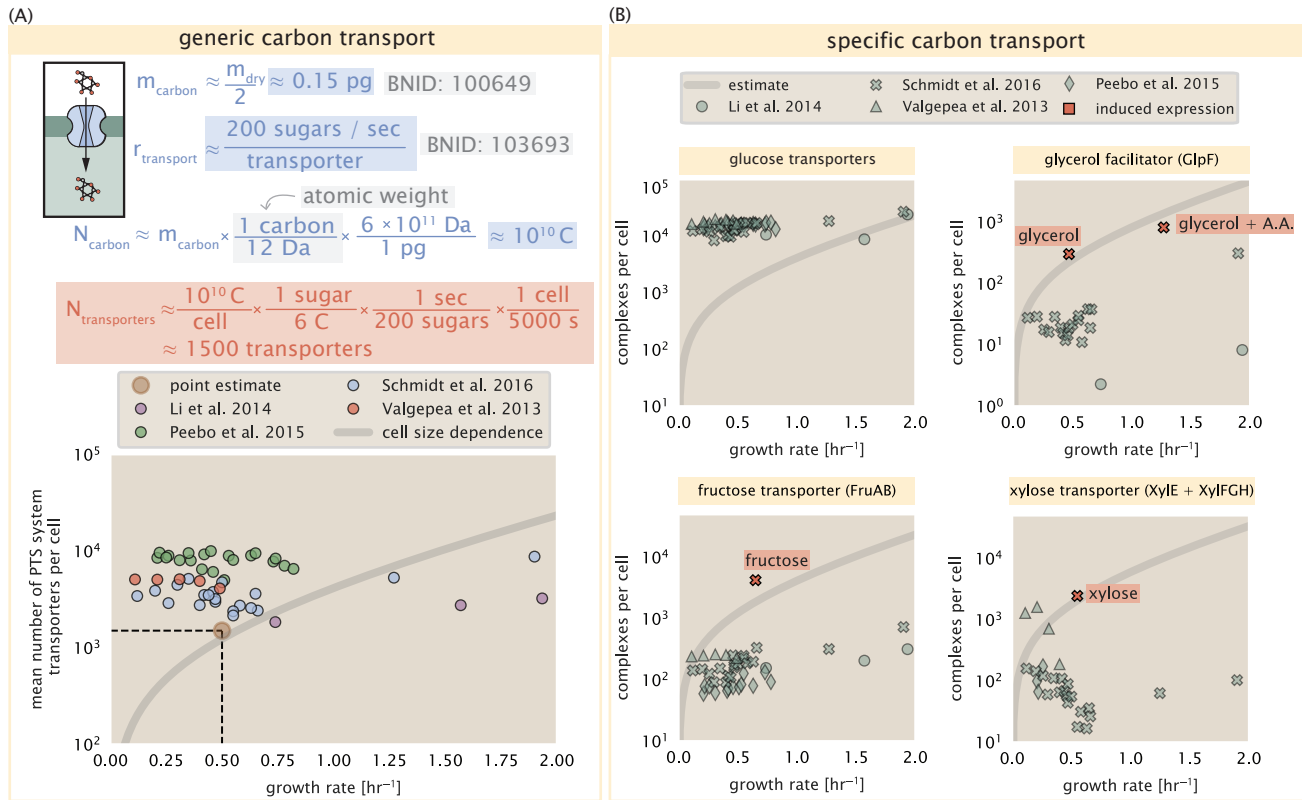


Figure 2. The abundance of carbon transport systems across growth rates. (A) A simple estimate for the minimum number of generic carbohydrate transport systems (top) assumes $\approx 10^{10}$ C are needed to complete division, each transported sugar contains ≈ 6 C, and each transporter conducts sugar molecules at a rate of ≈ 200 per second. Bottom plot shows the estimated number of transporters needed at a growth rate of ≈ 0.5 per hr (light-brown point and dashed lines). Colored points correspond to the mean number of PTS system sugar transporters (complexes annotated with the Gene Ontology term GO:0009401) for different growth conditions across different published datasets. (B) The abundance of various specific carbon transport systems plotted as a function of the population growth rate. The rates of substrate transport to compute the continuum growth rate estimate (grey line) were 200 glucose·s⁻¹ (BNID: 103693, *Milo et al. (2010)*), 2000 glycerol·s⁻¹ (*Lu et al., 2003*), 200 fructose·s⁻¹ (assumed to be similar to PtsI, BNID: 103693, *Milo et al. (2010)*), and 50 xylose·s⁻¹ (assumed to be comparable to LacY, BNID:103159, *Milo et al. (2010)*). Red points and highlighted text indicate conditions in which the only source of carbon in the growth medium induces expression of the transport system. Grey line in (A) and (B) represents the estimated number of transporters per cell at a continuum of growth rates.

166 show the estimated number of transporters needed at each growth rate to satisfy the cellular
 167 carbon requirement. It is notable that in all cases, the magnitude of induced expression (shown in
 168 red) falls close to the estimate, illustrating the ability of the cell to tune expression in response to
 169 changing environments. Together, this generic estimation and the specific examples of induced
 170 expression suggest that transport of carbon across the cell membrane, while critical for growth, is
 171 not the rate-limiting step of cell division.

172 **Phosphorus and Sulfur Transport**

173 We now turn our attention towards other essential elements, namely phosphorus and sulfur.
 174 Phosphorus is critical to the cellular energy economy in the form of high-energy phosphodiester
 175 bonds making up DNA, RNA, and the NTP energy pool as well as playing a critical role in the post-
 176 translational modification of proteins and defining the polar-heads of lipids. In total, phosphorus
 177 makes up $\approx 3\%$ of the cellular dry mass which in typical experimental conditions is in the form of
 178 inorganic phosphate. The cell membrane has remarkably low permeability to this highly-charged
 179 and critical molecule, therefore requiring the expression of active transport systems. In *E. coli*, the
 180 proton electrochemical gradient across the inner membrane is leveraged to transport inorganic
 181 phosphate into the cell (Rosenberg et al., 1977). Proton-solute symporters are widespread in *E.*
coli (Ramos and Kaback, 1977; Booth et al., 1979) and can have rapid transport rates of 50 to 100
 182 molecules per second for sugars and other solutes (BNID: 103159; 111777, Milo et al. (2010)). As
 183 a more extreme example, the proton transporters in the F₁-F₀ ATP synthase, which leverage the
 184 proton electrochemical gradient for rotational motion, can shuttle protons across the membrane at
 185 a rate of ≈ 1000 per second (BNID: 104890; 103390, (Milo et al., 2010)). In *E. coli* the PitA phosphate
 186 transport system has been shown to be very tightly coupled with the proton electrochemical
 187 gradient with a 1:1 proton:phosphate stoichiometric ratio (Harris et al., 2001; Feist et al., 2007).
 188 Taking the geometric mean of the aforementioned estimates gives a plausible rate of phosphate
 189 transport on the order of 300 per second. Illustrated in **Figure 3(A)**, we can estimate that ≈ 150
 190 phosphate transporters are necessary to maintain an $\approx 3\%$ dry mass with a 5000 s division time.
 191 This estimate is again satisfied when we examine the observed copy numbers of PitA in proteomic
 192 data sets (plot in **Figure 3(A)**). While our estimate is very much in line with the observed numbers,
 193 we emphasize that this is likely a slight overestimate of the number of transporters needed as there
 194 are other phosphorous scavenging systems, such as the ATP-dependent phosphate transporter Pst
 195 system which we have neglected.
 196

197 Satisfied that there are a sufficient number of phosphate transporters present in the cell, we
 198 now turn to sulfur transport as another potentially rate limiting process. Similar to phosphate,
 199 sulfate is highly-charged and not particularly membrane permeable, requiring active transport.
 200 While there exists a H+/sulfate symporter in *E. coli*, it is in relatively low abundance and is not well
 201 characterized (Zhang et al., 2014a). Sulfate is predominantly acquired via the ATP-dependent ABC
 202 transporter CysUWA system which also plays an important role in selenium transport (Sekowska
 203 et al., 2000; Sirko et al., 1995). While specific kinetic details of this transport system are not readily
 204 available, generic ATP transport systems in prokaryotes transport on the order of 1 to 10 molecules
 205 per second (BNID: 109035, Milo et al. (2010)). Combining this generic transport rate, measurement
 206 of sulfur comprising 1% of dry mass, and a 5000 second division time yields an estimate of \approx
 207 1000 CysUWA complexes per cell (**Figure 3(B)**). Once again, this estimate is in notable agreement
 208 with proteomic data sets, suggesting that there are sufficient transporters present to acquire the
 209 necessary sulfur. In a similar spirit of our estimate of phosphorus transport, we emphasize that
 210 this is likely an overestimate of the number of necessary transporters as we have neglected other
 211 sulfur scavenging systems that are in lower abundance.

212 **Limits on Transporter Expression**

213 So which, if any, of these processes may be rate limiting for growth? As suggested by **Figure 2**
 214 (B), induced expression can lead to an order-of-magnitude (or more) increase in the amount of

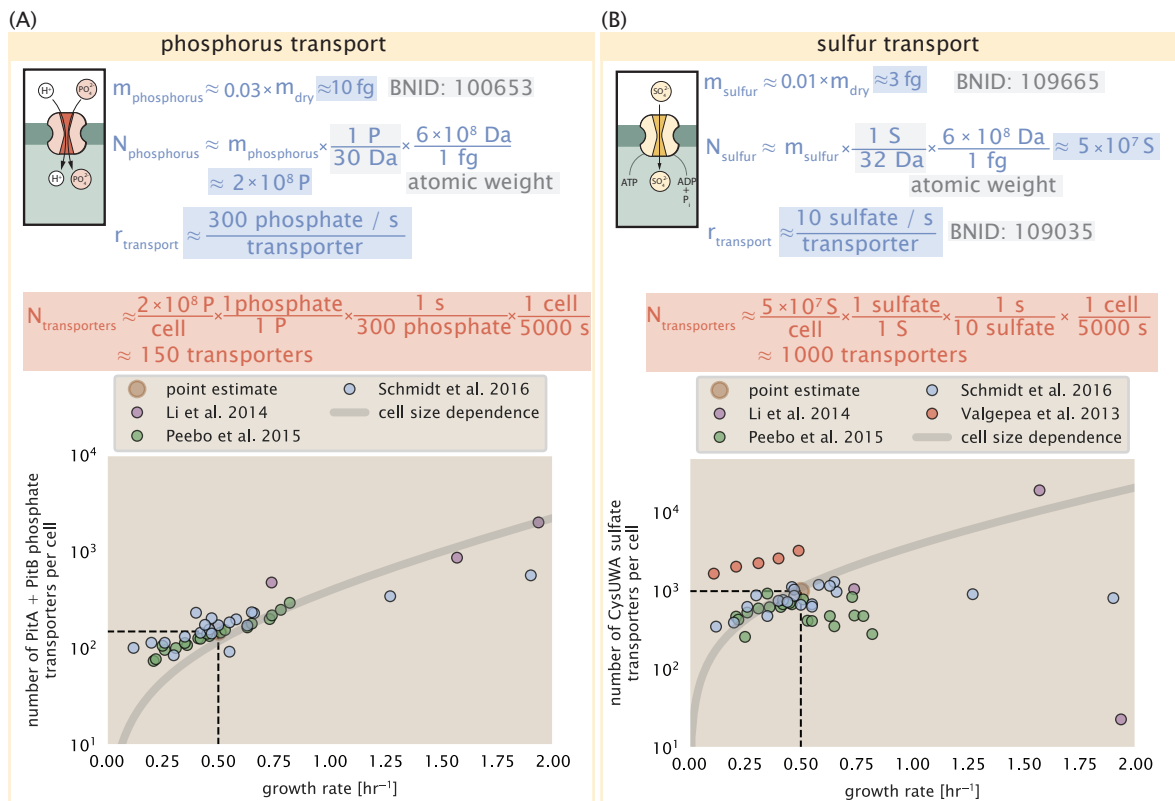


Figure 3. Estimates and measurements of phosphate and sulfate transport systems as a function of growth rate. (A) Estimate for the number of PitA phosphate transport systems needed to maintain a 3% phosphorus *E. coli* dry mass. Points in plot correspond to the total number of PitA transporters per cell. (B) Estimate of the number of CysUWA complexes necessary to maintain a 1% sulfur *E. coli* dry mass. Points in plot correspond to average number of CysUWA transporter complexes that can be formed given the transporter stoichiometry [CysA]₂[CysU][CysW][Sbp/CysP]. Grey line in (A) and (B) represents the estimated number of transporters per cell at a continuum of growth rates.

215 transporters needed to facilitate transport. Thus, if acquisition of nutrients was the limiting state
 216 in cell division, could expression simply be increased to accommodate faster growth? A way to
 217 approach this question is to compute the amount of space in the bacterial membrane that could be
 218 occupied by nutrient transporters. Considering a rule-of-thumb for the surface area of *E. coli* of
 219 about $6 \mu\text{m}^2$ (BNID: 101792, *Milo et al. (2010)*), we expect an areal density for 1000 transporters to
 220 be approximately 200 transporters/ μm^2 . For a typical transporter occupying about $50 \text{ nm}^2/\text{dimer}$,
 221 this amounts to about only 1 percent of the total inner membrane (*Szenk et al., 2017*). In addition,
 222 bacterial cell membranes typically have densities of 10^5 proteins/ μm^2 (*Phillips, 2018*), implying that
 223 the cell could accommodate more transporters of a variety of species if it were rate limiting. As we
 224 will see in the next section, however, occupancy of the membrane can impose other limits on the
 225 rate of energy production.

226 Energy Production

227 While the transport of nutrients is required to build new cell mass, the metabolic pathways both
 228 consume and generate energy in the form of NTPs. The high-energy phosphodiester bonds
 229 of (primarily) ATP power a variety of cellular processes that drive biological systems away from
 230 thermodynamic equilibrium. The next set of processes we hypothesize might control the rate of
 231 cell division considers the energy budget of a dividing cell in terms of the synthesis of ATP from
 232 ADP and inorganic phosphate as well as maintenance of the electrochemical proton gradient which
 233 powers it.

234 ATP Synthesis

235 Hydrolysis of the terminal phosphodiester bond of ATP forming ADP and an inorganic phosphate is
 236 a kinetic driving force in a wide array of biochemical reactions. One such reaction is the formation
 237 of peptide bonds during translation which requires ≈ 2 ATPs for the charging of an amino acid to
 238 the tRNA and ≈ 2 ATP equivalents for the formation of the peptide bond between amino acids.
 239 Considering the ATP costs associated with error correction and post-translational modifications
 240 of proteins, we can make the approximation that each peptide bond has a net cost of ≈ 5 ATP
 241 (BNID: 107782, *Milo et al. (2010)*). In total, the energetic costs of peptide bond formation consume
 242 $\approx 80\%$ of the cells ATP budget (BNID: 107782; 106158; 101637; 111918, *Milo et al. (2010); Lynch*
and Marinov (2015); Stouthamer (1973)). The pool of ATP is produced by the F₁-F₀ ATP synthase – a
 244 membrane-bound rotary motor which under ideal conditions can yield ≈ 300 ATP per second (BNID:
 245 114701; *Milo et al. (2010); Weber and Senior (2003)*).

246 To estimate the total number of ATP equivalents consumed during a cell cycle, we will make the
 247 approximation that there are $\approx 3 \times 10^6$ proteins per cell with an average protein length of ≈ 300
 248 peptide bonds (BNID: 115702; 108986; 104877, *Milo et al. (2010)*). Taking these values together,
 249 we estimate that the typical *E. coli* cell consumes $\approx 5 \times 10^9$ ATP per cell cycle on protein synthesis
 250 alone and $\approx 6 \times 10^9$ ATP in total. Assuming that the ATP synthases are operating at their fastest
 251 possible rate, ≈ 3000 ATP synthases are needed to keep up with the energy demands of the cell.
 252 This estimate and a comparison with the data are shown in *Figure 4* (A). Despite our assumption of
 253 maximal ATP production rate per synthase and approximation of all NTP consuming reactions being
 254 the same as ATP, we find that an estimate of a few thousand complete synthases per cell to agree
 255 well with the experimental data. Much as we did for the estimates of transporter copy number in
 256 the previous section, we can generalize this estimation to consider a continuum of growth rates
 257 rather than a point estimate of 5000 s, indicated by the gray lines in *Figure 4*, and find that this
 258 approach adequately describes the observed growth rate dependence.

259 If the direct production of ATP was a rate limiting step for growth, could the cell simply express
 260 more ATP synthase complexes? This requires us to consider several features of cellular physiology,
 261 namely the physical space on the inner membrane as well as the ability to maintain the proton
 262 chemical gradient leveraged by the synthase to drive ATP production out of equilibrium.

263 **Generating the Proton Electrochemical Gradient**

264 In order to produce ATP, the F₁-F₀ ATP synthase itself must consume energy. Rather than burning
 265 through its own product, this intricate macromolecular machine has evolved to exploit the elec-
 266 trochemical potential established across the inner membrane through cellular respiration. This
 267 electrochemical gradient is manifest by the pumping of protons into the intermembrane space via
 268 the electron transport chains as they reduce NADH. In *E. coli*, this potential difference is ≈ -200 mV
 269 (BNID: 102120, *Milo et al. (2010)*). A simple estimate of the inner membrane as a capacitor with a
 270 working voltage of -200 mV (as performed in the Supplemental Information) reveals that $\approx 2 \times 10^4$
 271 protons must be present in the intermembrane space.

272 However, the constant rotation of the ATP synthases would rapidly abolish this potential differ-
 273 ence if it were not being actively maintained. To undergo a complete rotation (and produce a single
 274 ATP), the F₁-F₀ ATP synthase must shuttle ≈ 4 protons across the membrane into the cytosol (BNID:
 275 103390, *Milo et al. (2010)*). With ≈ 3000 ATP synthases each generating 300 ATP per second, the
 276 2×10^4 protons establishing the 200 mV potential would be consumed in only a few milliseconds.
 277 This brings us to our next estimate: how many electron transport complexes are needed to support
 278 the consumption rate of the ATP synthases?

279 The electrochemistry of the electron transport complexes of *E. coli* have been the subject of
 280 intense biochemical and biophysical study over the past half century (*Ingledew and Poole, 1984;*
 281 *Khademian and Imlay, 2017; Cox et al., 1970; Henkel et al., 2014*). A recent work (*Szenk et al.,*
 282 *2017*) examined the respiratory capacity of the *E. coli* electron transport complexes using structural
 283 and biochemical data, revealing that each electron transport chain rapidly pumps protons into
 284 the intermembrane space at a clip of ≈ 1500 protons per second (BNID: 114704; 114687, *Milo*
 285 *et al. (2010)*). Using our estimate of the number of ATP synthases required per cell (*Figure 4(A)*),
 286 coupled with these recent measurements, we estimate that ≈ 1000 electron transport complexes
 287 would be necessary to facilitate the $\approx 4 \times 10^6$ protons per second diet of the cellular ATP synthases.
 288 This estimate (along with a generalization to the entire range of observed growth rates) is in
 289 agreement with the number of complexes identified in the proteomic datasets (plot in *Figure 4(B)*).
 290 This suggests that every ATP synthase must be accompanied by ≈ 1 functional electron transport
 291 chain. Again, if this were a rate limiting process for bacterial growth, one must conclude that it is
 292 not possible for the cell to simply increase the production of both the number of electron transport
 293 chain complexes as well as ATP synthases. As both of these components only function bound to
 294 the inner membrane, we now turn our attention towards the available space in the membrane as
 295 well as surface-area-to-volume constraints.

296 **Energy Production in a Crowded Membrane.**

297 For each protein considered so far, the data shows that in general their numbers increase with
 298 growth rate. This is in part a consequence of the increase in cell length and width at that is common
 299 to many rod-shaped bacteria at faster growth rates (*Ojikic et al., 2019; Harris and Theriot, 2018*).
 300 For the particular case of *E. coli*, the total cellular protein and cell size increase logarithmically
 301 with growth rate (*Schaechter et al., 1958; Si et al., 2017*). Indeed, this is one reason why we have
 302 considered only a single, common growth condition across all our estimates so far. Such a scaling
 303 will require that the total number of proteins and net demand on resources also grow in proportion
 304 to the increase in cell size divided by the cell's doubling time. Recall however that each transport
 305 process, as well as the ATP production via respiration, is performed at the bacterial membrane. This
 306 means that their maximum productivity can only increase in proportion to the cell's surface area
 307 divided by the cell doubling time. This difference in scaling would vary in proportion to the surface
 308 area-to-volume (S/V) ratio.

309 While we found that there was more than sufficient membrane real estate for carbon intake in
 310 our earlier estimate, the total number of ATP synthases and electron chain transport complexes
 311 both exhibit a clear increase in copy number with growth rate, reaching in excess of 10^4 copies per
 312 cell (*Figure 4*). Here we consider the consequences of this S/V ratio scaling in more detail.

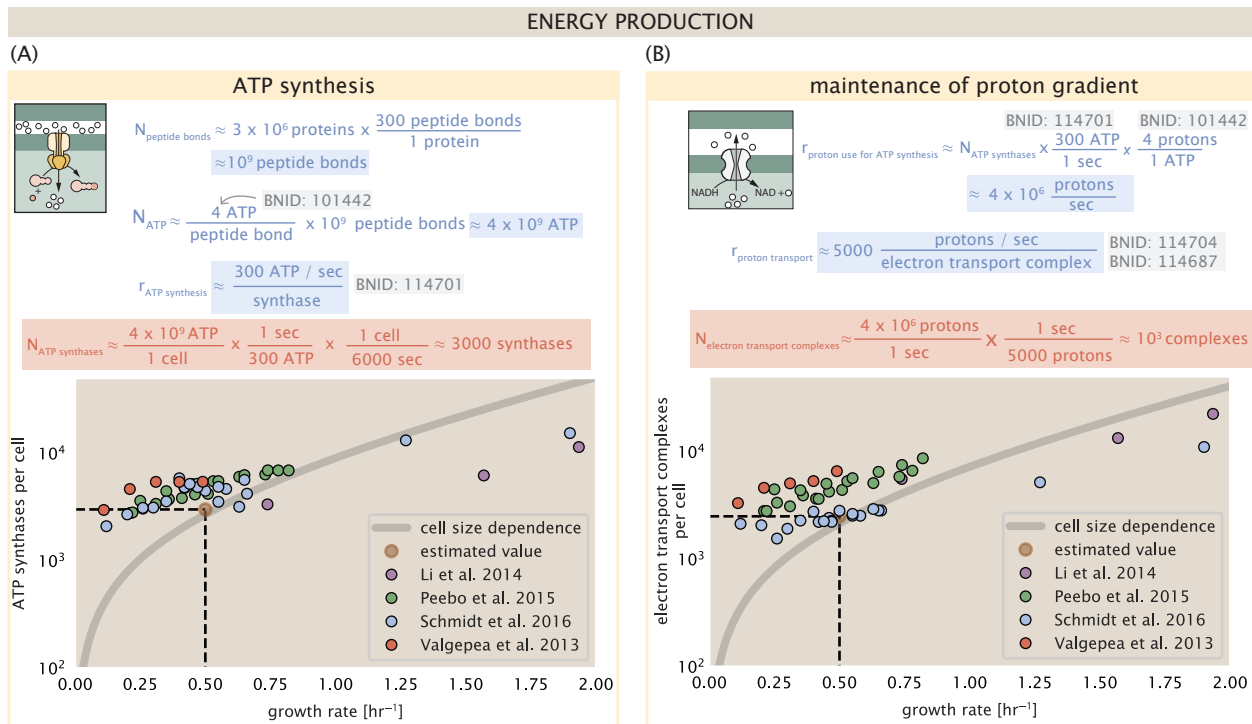


Figure 4. The abundance of F₁-F₀ ATP synthases and electron transport chain complexes as a function of growth rate. (A) Estimate of the number of F₁-F₀ ATP synthase complexes needed to accommodate peptide bond formation and other NTP dependent processes. Points in plot correspond to the mean number of complete F₁-F₀ ATP synthase complexes that can be formed given proteomic measurements and the subunit stoichiometry [AtpE]₁₀[AtpF]₂[AtpB][AtpC][AtpH][AtpA]₃[AtpG][AtpD]₃. (B) Estimate of the number of electron transport chain complexes needed to maintain a membrane potential of ~ -200 mV given estimate of number of F₁-F₀ ATP synthases from (A). Points in plot correspond to the average number of complexes identified as being involved in aerobic respiration by the Gene Ontology identifier GO:0019646 that could be formed given proteomic observations. These complexes include cytochromes *bd1* ([CydA][CydB][CydX][CydH]), *bdII* ([AppC][AppB]), *bo3*, ([CyoD][CyoA][CyoB][CyoC]) and NADH:quinone oxidoreductase I ([NuoA][NuoH][NuoJ][NuoK][NuoL][NuoM][NuoN][NuoB][NuoC][NuoE][NuoF][NuoG][NuoI]) and II ([Ndh]). Grey lines in both (A) and (B) correspond to the estimate procedure described, but applied to a continuum of growth rates. We direct the reader to the Supporting Information for a more thorough description of this approach.

313 In our estimate of ATP production above we found that a cell demands about 6×10^9 ATP or
 314 10^6 ATP/s. With a cell volume of roughly 1 fL, this corresponds to about 2×10^{10} ATP per fL of cell
 315 volume, in line with previous estimates (*Stouthamer and Bettenhausen, 1977; Szenk et al., 2017*).
 316 In **Figure 5** (A) we plot this ATP demand as a function of the S/V ratio in green, where we have
 317 considered a range of cell shapes from spherical to rod-shaped with an aspect ratio (length/width)
 318 equal to 4 (See appendix for calculations of cell volume and surface area). In order to consider the
 319 maximum power that could be produced, we consider the amount of ATP that can be generated by a
 320 membrane filled with ATP synthase and electron transport complexes, which provides a maximal
 321 production of about 3 ATP / (nm²·s) (*Szenk et al., 2017*). This is shown in blue in **Figure 5**(A), which
 322 shows that at least for the growth rates observed, the energy demand is roughly an order of
 323 magnitude less.

324 Interestingly, *Szenk et al. (2017)* also found that ATP production by respiration is less efficient
 325 than by fermentation per membrane area occupied due to the additional proteins of the electron
 326 transport chain. This suggests that even under anaerobic growth, there will be sufficient membrane
 327 space for ATP production in general.

328 While this serves to highlight the diminishing capacity to provide resources to grow if the cell
 329 increases in size (and its S/V decreases), the blue region in **Figure 5**(A) represents a somewhat
 330 unachievable limit since the inner membrane must also include other proteins such as those
 331 required for lipid and membrane synthesis. To gain insight, we used the proteomic data to look at
 332 the distribution of proteins on the inner membrane. Here we use Gene Ontology (GO) annotations
 333 (*Ashburner et al., 2000; The Gene Ontology Consortium, 2018*) to identify all proteins embedded or
 334 peripheral to the inner membrane (GO term: 0005886). Those associated but not membrane-bound
 335 include proteins like MreB and FtsZ, that traverse the inner membrane by treadmilling and must
 336 nonetheless be considered as a vital component occupying space on the membrane. In **Figure 5** (B),
 337 we find that the total protein mass per μm^2 is relatively constant with growth rate. Interestingly,
 338 when we consider the distribution of proteins grouped by their Clusters of Orthologous Groups
 339 (COG) (*Tatusov et al., 2000*), the relative abundance for those in metabolism (including ATP synthesis
 340 via respiration) is also relatively constant.

341 Function of the Central Dogma

342 Up to this point, we have considered a variety of transport and biosynthetic processes that are
 343 critical to acquiring and generating new cell mass. While there are of course many other metabolic
 344 processes we could consider and perform estimates of (such as the components of fermentative
 345 versus aerobic respiration), we now turn our focus to some of the most central processes which
 346 must be undertaken irrespective of the growth conditions – the processes of the central dogma.

347 DNA

348 Most bacteria (including *E. coli*) harbor a single, circular chromosome and can have extra-chromosomal
 349 plasmids up to ~ 100 kbp in length. We will focus our quantitative thinking solely on the chromo-
 350 some of *E. coli* which harbors ≈ 5000 genes and $\approx 5 \times 10^6$ base pairs. To successfully divide and
 351 produce viable progeny, this chromosome must be faithfully replicated and segregated into each
 352 nascent cell. We again rely on the near century of literature in molecular biology to provide some
 353 insight on the rates and mechanics of the replicative feat as well as the production of the required
 354 starting materials, dNTPs.

355 dNTP synthesis

356 We begin our exploration DNA replication by examining the production of the deoxyribonucleotide
 357 triphosphates (dNTPs). The four major dNTPs (dATP, dTTP, dCTP, and dGTP) are synthesized *de novo*
 358 in separate pathways, requiring different building blocks. However, a critical step present in all
 359 dNTP synthesis pathways is the conversion from ribonucleotide to deoxyribonucleotide via the
 360 removal of the 3' hydroxyl group of the ribose ring (*Rudd et al., 2016*). This reaction is mediated by a

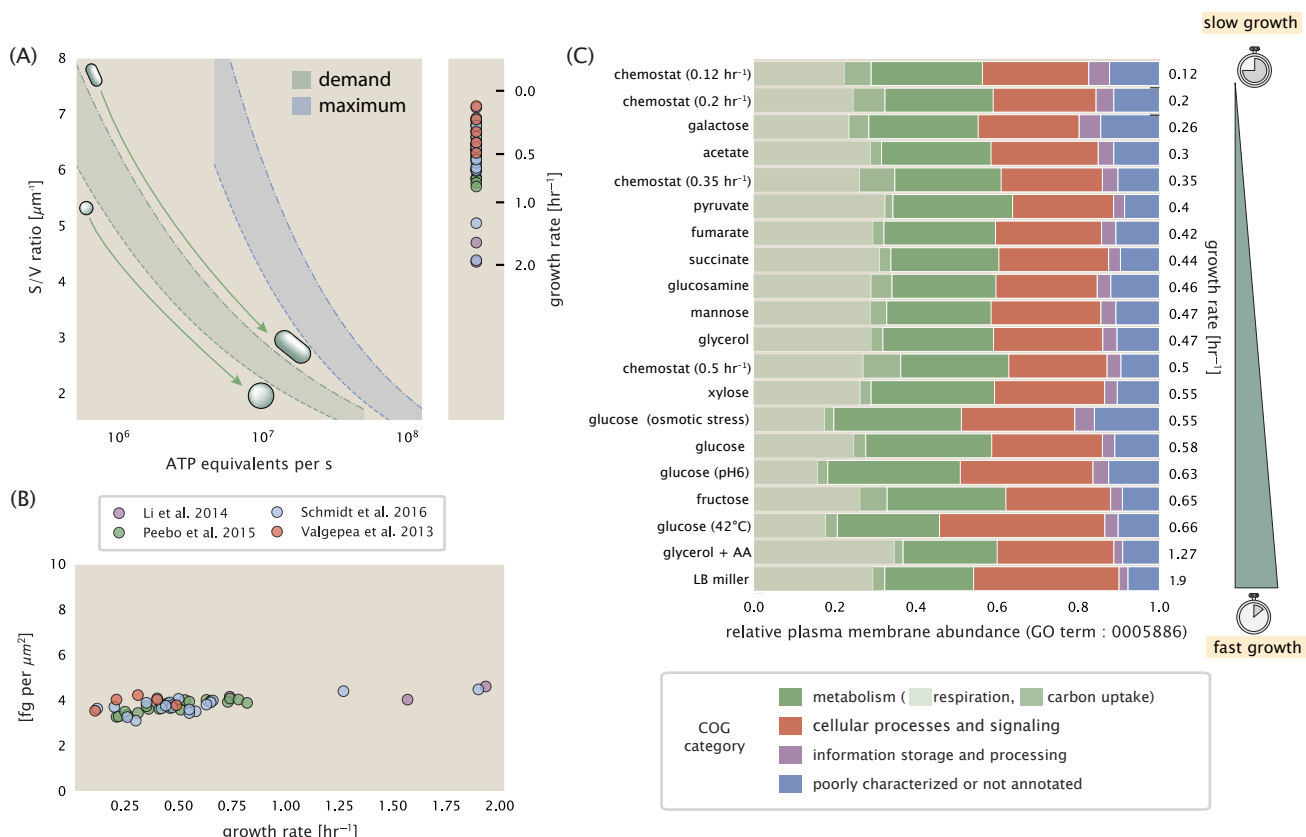


Figure 5. Influence of cell size and S/V ratio on ATP production and inner membrane composition. (A) Scaling of ATP demand and maximum ATP production as a function of S/V ratio. Cell volumes of 0.5 fL to 50 fL were considered, with the dashed (—) line corresponding to a sphere and the dash-dot line (---) reflecting a rod-shaped bacterium like *E. coli* with a typical aspect ratio (length / width) of 0.4 (Shi et al., 2018). Approximately 50% of the bacterial inner membrane is assumed to be protein, with the remainder lipid. (B) Total protein mass calculated for proteins with inner membrane annotation (GO term: 0005886). (C) Relative protein abundances by mass based on COG annotation. Metabolic proteins are further separated into respiration (F_1 - F_0 ATP synthase, NADH dehydrogenase I, succinate:quinone oxidoreductase, cytochrome b o₃ ubiquinol oxidase, cytochrome bd-I ubiquinol oxidase) and carbohydrate transport (GO term: GO:0008643). Note that the elongation factor EF-Tu can also associate with the inner membrane, but was excluded in this analysis due to its high relative abundance (roughly identical to the total mass shown in part (B)).

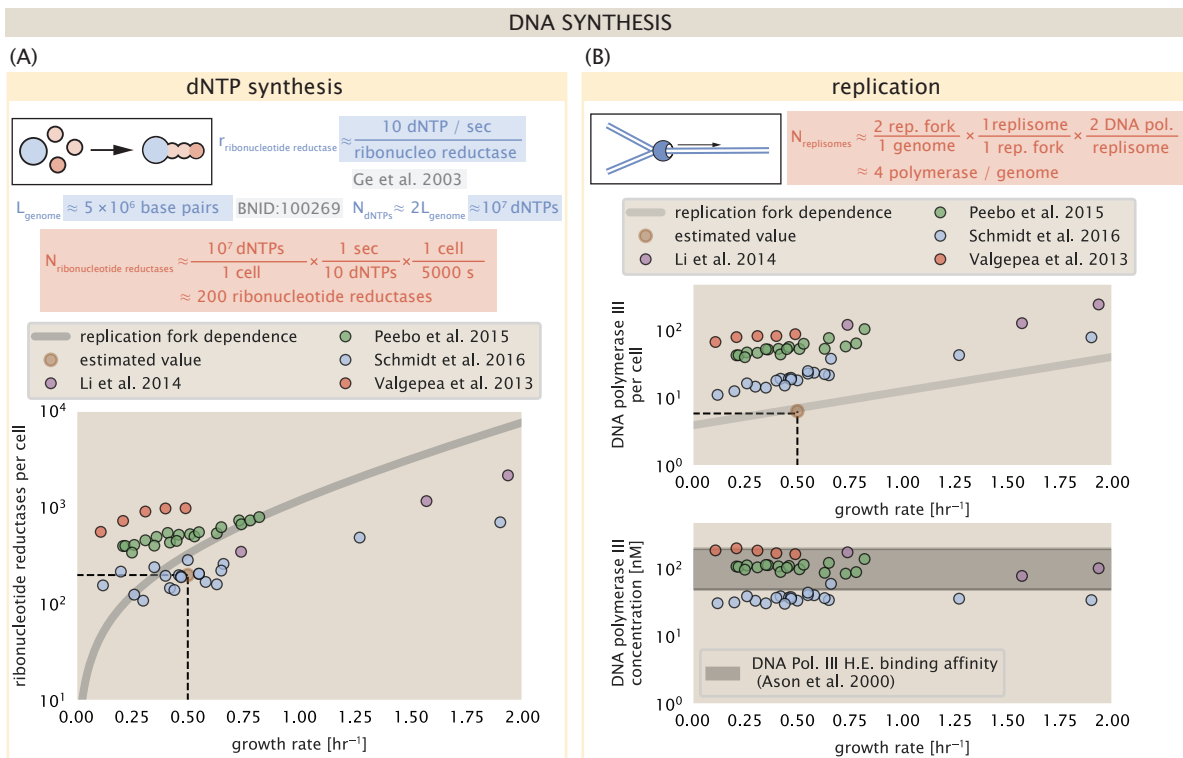


Figure 6. Complex abundance estimates for dNTP synthesis and DNA replication. (A) Estimate of the number of ribonucleotide reductase enzymes needed to facilitate the synthesis of $\approx 10^7$ dNTPs over the course of a 5000 second generation time. Points in the plot correspond to the total number of ribonucleotide reductase I ($[NrdA]_2[NrdB]_2$) and ribonucleotide reductase II ($[NrdE]_2[NrdF]_2$) complexes. (B) An estimate for the minimum number of DNA polymerase holoenzyme complexes needed to facilitate replication of a single genome. Points in the top plot correspond to the total number of DNA polymerase III holoenzyme complexes ($[DnaE]_3[DnaQ]_3[HolE]_3[DnaX]_5[HolB][HolA][DnaN]_4[HolC]_4[HolD]_4$) per cell. Bottom plot shows the effective concentration of DNA polymerase III holoenzyme given cell volumes calculated from the growth rate as in *Sj et al. (2019)* (See Supplemental Information Section 4). Grey lines in (A) and top panel of (B) show the estimated number of complexes needed as a function of growth, the details of which are described in the Supplemental Information.

361 class of enzymes termed ribonucleotide reductases, of which *E. coli* possesses two aerobically active
 362 complexes (termed I and II) and a single anaerobically active enzyme. Due to their peculiar formation
 363 of a radical intermediate, these enzymes have received much biochemical, kinetic, and structural
 364 characterization. One such work (*Ge et al., 2003*) performed a detailed *in vitro* measurement of the
 365 steady-state kinetic rates of these complexes, revealing a turnover rate of ≈ 10 dNTP per second.

366 Since this reaction is central to the synthesis of all dNTPs, it is reasonable to consider the
 367 abundance of these complexes is a measure of the total dNTP production in *E. coli*. Illustrated
 368 schematically in *Figure 6* (A), we consider the fact that to replicate the cell's genome, on the order of
 369 $\approx 10^7$ dNTPs must be synthesized. Assuming a production rate of 10 per second per ribonucleotide
 370 reductase complex and a cell division time of 5000 seconds, we arrive at an estimate of ≈ 200
 371 complexes needed per cell. As shown in the bottom panel of *Figure 6* (A), this estimate agrees
 372 with the experimental measurements of these complexes abundances within $\approx 1/2$ an order of
 373 magnitude. Extension of this estimate across a continuum of growth rate, including the fact that
 374 multiple chromosomes can be replicated at a given time, is shown as a grey transparent line in
 375 *Figure 6* (A). Similarly to our point estimate, this refinement agrees well with the data, accurately
 376 describing both the magnitude of the complex abundance and the dependence on growth rate.

377 Recent work has revealed that during replication, the ribonucleotide reductase complexes
 378 coalesce to form discrete foci colocalized with the DNA replisome complex (*Sánchez-Romero et al.,*
 379 *2011*). This is particularly pronounced in conditions where growth is slow, indicating that spatial
 380 organization and regulation of the activity of the complexes plays an important role.

381 DNA Replication

382 We now turn our focus to the integration of these dNTP building blocks into the replicated chromo-
 383 some strand via the DNA polymerase. Replication is initiated at a single region of the chromosome
 384 termed the *oriC* locus at which a pair of DNA polymerases bind and begin their high-fidelity replica-
 385 tion of the genome in opposite directions. Assuming equivalence between the two replication forks,
 386 this means that the two DNA polymerase complexes (termed replisomes) meet at the midway point
 387 of the circular chromosome termed the *ter* locus. The kinetics of the five types of DNA polymerases
 388 (I – V) have been intensely studied, revealing that DNA polymerase III performs the high fidelity
 389 processive replication of the genome with the other "accessory" polymerases playing auxiliary roles
 390 (*Fijalkowska et al., 2012*). *In vitro* measurements have shown that DNA Polymerase III copies DNA
 391 at a rate of \approx 600 nucleotides per second (BNID: 104120, *Milo et al. (2010)*). Therefore, to replicate
 392 a single chromosome, two replisomes (containing two DNA polymerase III each) moving at their
 393 maximal rate would copy the entire genome in \approx 4000 s. Thus, with a division time of 5000 s (our
 394 "typical" growth rate for the purposes of this work), there is sufficient time for a pair of replisomes
 395 complexes to replicate the entire genome. However, this estimate implies that 4000 s would be the
 396 upper-limit time scale for bacterial division which is at odds with the familiar 20 minute (1200 s)
 397 doubling time of *E. coli* in rich medium.

398 It is well known that *E. coli* can parallelize its DNA replication such that multiple chromosomes
 399 are being replicated at once, with as many as 10 - 12 replication forks at a given time (*Bremer*
 400 and *Dennis, 2008*; *Si et al., 2017*). Thus, even in rapidly growing cultures, we expect only a few
 401 polymerases (\approx 10) are needed to replicate the chromosome per cell doubling. However, as shown
 402 in *Figure 6(B)*, DNA polymerase III is nearly an order of magnitude more abundant. This
 403 discrepancy can be understood by considering its binding constant to DNA. DNA polymerase III
 404 is highly processive, facilitated by a strong affinity of the complex to the DNA. *In vitro* biochemical
 405 characterization has quantified the K_D of DNA polymerase III holoenzyme to single-stranded and
 406 double-stranded DNA to be 50 and 200 nM, respectively (*Ason et al., 2000*). The bottom plot in
 407 *Figure 6* (B) shows that the concentration of the DNA polymerase III across all data sets and growth
 408 conditions is within this range. Thus, while the copy number of the DNA polymerase III is in excess
 409 of the strict number required to replicate the genome, its copy number appears to vary such that its
 410 concentration is approximately equal to the dissociation constant to the DNA. While the processes
 411 regulating the initiation of DNA replication are complex and involve more than just the holoenzyme,
 412 these data indicate that the kinetics of replication rather than the explicit copy number of the DNA
 413 polymerase III holoenzyme is the more relevant feature of DNA replication to consider. In light
 414 of this, the data in *Figure 6(B)* suggests that for bacteria like *E. coli*, DNA replication does not represent a rate-limiting step in cell division. However, it is worth noting that for bacterium like *C. crescentus* whose chromosomal replication is initiated only once per cell cycle (*Jensen et al., 2001*), the time to double their chromosome likely represents an upper limit to their growth rate.

418 RNA Synthesis

419 With the machinery governing the replication of the genome accounted for, we now turn our
 420 attention to the next stage of the central dogma – the transcription of DNA to form RNA. We
 421 primarily consider three major groupings of RNA, namely the RNA associated with ribosomes
 422 (rRNA), the RNA encoding the amino-acid sequence of proteins (mRNA), and the RNA which links
 423 codon sequence to amino-acid identity during translation (tRNA). Despite the varied function of
 424 these RNA species, they share a commonality in that they are transcribed from DNA via the action
 425 of RNA polymerase. In the coming paragraphs, we will consider the synthesis of RNA as a rate
 426 limiting step in bacterial division by estimating how many RNA polymerases must be present to
 427 synthesize all necessary rRNA, mRNA, and tRNA.

428 rRNA

429 We begin with an estimation of the number of RNA polymerases needed to synthesize the rRNA
 430 that serve as catalytic and structural elements of the ribosome. Each ribosome contains three rRNA
 431 molecules of lengths 120, 1542, and 2904 nucleotides (BNID: 108093, *Milo et al. (2010)*), meaning
 432 each ribosome contains \approx 4500 nucleotides. As the *E. coli* RNA polymerase transcribes DNA to RNA
 433 at a rate of \approx 40 nucleotides per second (BNID: 101904, *Milo et al. (2010)*), it takes a single RNA
 434 polymerase \approx 100 s to synthesize the RNA needed to form a single functional ribosome. Therefore,
 435 in a 5000 s division time, a single RNA polymerase transcribing rRNA at a time would result in only
 436 \approx 50 functional ribosomal rRNA units – far below the observed number of \approx 10^4 ribosomes per cell.

437 Of course, there can be more than one RNA polymerase transcribing the rRNA genes at any
 438 given time. To elucidate the *maximum* number of rRNA units that can be synthesized given a single
 439 copy of each rRNA gene, we will consider a hypothesis in which the rRNA operon is completely tiled
 440 with RNA polymerase. *In vivo* measurements of the kinetics of rRNA transcription have revealed that
 441 RNA polymerases are loaded onto the promoter of an rRNA gene at a rate of \approx 1 per second (BNID:
 442 111997; 102362, *Milo et al. (2010)*). If RNA polymerases are being constantly loaded on to the rRNA
 443 genes at this rate, then we can assume that \approx 1 functional rRNA unit is synthesized per second.
 444 With a 5000 second division time, this hypothesis leads to a maximal value of 5000 functional rRNA
 445 units, still undershooting the observed number of 10^4 ribosomes per cell.

446 *E. coli* has evolved a clever mechanism to surpass this kinetic limit for the rate of rRNA production.
 447 Rather than having only one copy of each rRNA gene, *E. coli* has seven copies of the operon
 448 (BIND: 100352, *Milo et al. (2010)*) four of which are localized directly adjacent to the origin of
 449 replication (*Birnbaum and Kaplan, 1971*). As fast growth also implies an increased gene dosage due
 450 to parallelized chromosomal replication, the total number of rRNA genes can be on the order of \approx
 451 10 – 70 copies at moderate to fast growth rates (*Stevenson and Schmidt, 2004*). Using our standard
 452 time scale of a 5000 second division time, we can make the lower-bound estimate that the typical
 453 cell will have 7 copies of the rRNA operon. Synthesizing one functional rRNA unit per second per
 454 rRNA operon, a total of 4×10^4 rRNA units can be synthesized, comfortably above the observed
 455 number of ribosomes per cell.

456 How many RNA polymerases are then needed to constantly transcribe 7 copies of the rRNA
 457 genes? We approach this estimate by considering the maximum number of RNA polymerases tiled
 458 along the rRNA genes with a loading rate of 1 per second and a transcription rate of 40 nucleotides
 459 per second. Considering that a RNA polymerase has a physical footprint of approximately 40
 460 nucleotides (BNID: 107873, *Milo et al. (2010)*), we can expect \approx 1 RNA polymerase per 80 nucleotides.
 461 With a total length of \approx 4500 nucleotides per operon and 7 operons per cell, the maximum number
 462 of RNA polymerases that can be transcribing rRNA at any given time is \approx 400. As we will see in the
 463 coming sections, the synthesis of rRNA is the dominant requirement of the RNA polymerase pool.

464 mRNA

465 To form a functional protein, all protein coding genes must first be transcribed from DNA to form
 466 an mRNA molecule. While each protein requires an mRNA blueprint, many copies of the protein
 467 can be synthesized from a single mRNA. Factors such as strength of the ribosomal binding site,
 468 mRNA stability, and rare codon usage frequency dictate the number of proteins that can be made
 469 from a single mRNA, with yields ranging from 10^1 to 10^4 (BNID: 104186; 100196; 106254, *Milo et al.*
 470 (2010)). Computing the geometric mean of this range yields \approx 1000 proteins synthesized per mRNA,
 471 a value that agrees with experimental measurements of the number of proteins per cell ($\approx 3 \times 10^6$,
 472 BNID: 100088, *Milo et al. (2010)*) and total number of mRNA per cell ($\approx 3 \times 10^3$, BNID: 100064, *Milo*
 473 *et al. (2010)*).

474 This estimation captures the *steady-state* mRNA copy number, meaning that at any given time,
 475 there will exist approximately 3000 unique mRNA molecules. To determine the *total* number of
 476 mRNA that need to be synthesized over the cell's lifetime, we must consider degradation of the
 477 mRNA. In most bacteria, mRNAs are rather unstable with life times on the order of several minutes

(BNID: 104324; 106253; 111927; 111998, *Milo et al. (2010)*). For convenience, we assume that the typical mRNA in our cell of interest has a typical lifetime of \approx 300 seconds. Using this value, we can determine the total mRNA production rate to maintain a steady-state copy number of 3000 mRNA per cell. While we direct the reader to the appendix for a more detailed discussion of mRNA transcriptional dynamics, we state here that the total mRNA production rate must be on the order of \approx 15 mRNA per second. In *E. coli*, the average protein is \approx 300 amino acids in length (BNID: 108986; *Milo et al. (2010)*), meaning that the corresponding mRNA is \approx 900 nucleotides which we will further approximate as \approx 1000 nucleotides to account for the non-protein coding regions on the 5' and 3' ends. This means that the cell must have enough RNA polymerase molecules about to sustain a transcription rate of \approx 1.5×10^4 nucleotides per second. Knowing that a single RNA polymerase polymerizes RNA at a clip of 40 nucleotides per second, we arrive at a comfortable estimate of \approx 250 RNA polymerase complexes needed to satisfy the mRNA demands of the cell. It is worth noting that this number is approximately half of that required to synthesize enough rRNA, as we saw in the previous section. We find this to be a striking result as these 250 RNA polymerase molecules are responsible for the transcription of the \approx 4000 protein coding genes that are not ribosome associated.

494 tRNA

495 The final class of RNA molecules worthy of quantitative consideration is the the pool of tRNAs
 496 used during translation to map codon sequence to amino acid identity. Unlike mRNA or rRNA,
 497 each individual tRNA is remarkably short, ranging from 70 to 95 nucleotides each (BNID: 109645;
 498 102340, *Milo et al. (2010)*). What they lack in length, they make up for in abundance. There are
 499 many measurements of the size of the *E. coli* tRNA pool, ranging from \approx 6×10^4 (BNID:105280, *Milo*
 500 *et al. (2010)*) to \approx 4×10^5 (BNID: 108611). To test tRNA synthesis as a possible growth-rate limiting
 501 stage, we will err towards a higher abundance of \approx 4×10^5 per cell. Combining the abundance and
 502 tRNA length measurements, we make the estimate that \approx 5×10^7 nucleotides are sequestered in
 503 tRNA per cell. Unlike mRNA, tRNA is remarkably stable with typical lifetimes *in vivo* on the order of
 504 \approx 48 hours (*Abelson et al., 1974; Svenningsen et al., 2017*) – well beyond the timescale of division.
 505 Once again using our rule-of-thumb for the rate of transcription to be 40 nucleotides per second
 506 and assuming a division time of \approx 5000 seconds, we arrive at an estimate of \approx 150 RNA polymerases
 507 to synthesize enough tRNA. This requirement pales in comparison to the number of polymerases
 508 needed to generate the rRNA and mRNA pools and can be neglected as a significant transcriptional
 509 burden.

510 RNA Polymerase and σ -factor Abundance

511 These estimates, summarized in *Figure 7* (A), reveal that synthesis of rRNA and mRNA are the dominant
 512 RNA species synthesized by RNA polymerase, suggesting the need for \approx 700 RNA polymerases
 513 per cell. As is revealed in *Figure 7* (B), this estimate is about an order of magnitude below the observed
 514 number of RNA polymerase complexes per cell (\approx 5000 - 7000). The disagreement between the estimated
 515 number of RNA polymerases and these observations are at least consistent with recent literature revealing
 516 that \approx 80 % of RNA polymerases in *E. coli* are not transcriptionally active (*Patrick et al., 2015*). Our estimate ignores the possibility that some fraction is only nonspecifically
 517 bound to DNA, as well as the obstacles that RNA polymerase and DNA polymerase present for each
 518 other as they move along the DNA (*Finkelstein and Greene, 2013*).

519 In addition, it is also vital to consider the role of σ -factors which help RNA polymerase identify
 520 and bind to transcriptional start sites (*Browning and Busby, 2016*). Here we consider σ^{70} (RpoD)
 521 which is the dominant "general-purpose" σ -factor in *E. coli*. While initially thought of as being solely
 522 involved in transcriptional initiation, the past two decades of single-molecule work has revealed
 523 a more multipurpose role for σ^{70} including facilitating transcriptional elongation (*Kapanidis et al., 2005; Goldman et al., 2015; Perdue and Roberts, 2011; Mooney and Landick, 2003; Mooney et al., 2005*). *Figure 7* (B) is suggestive of such a role as the number of σ^{70} proteins per cell is in close

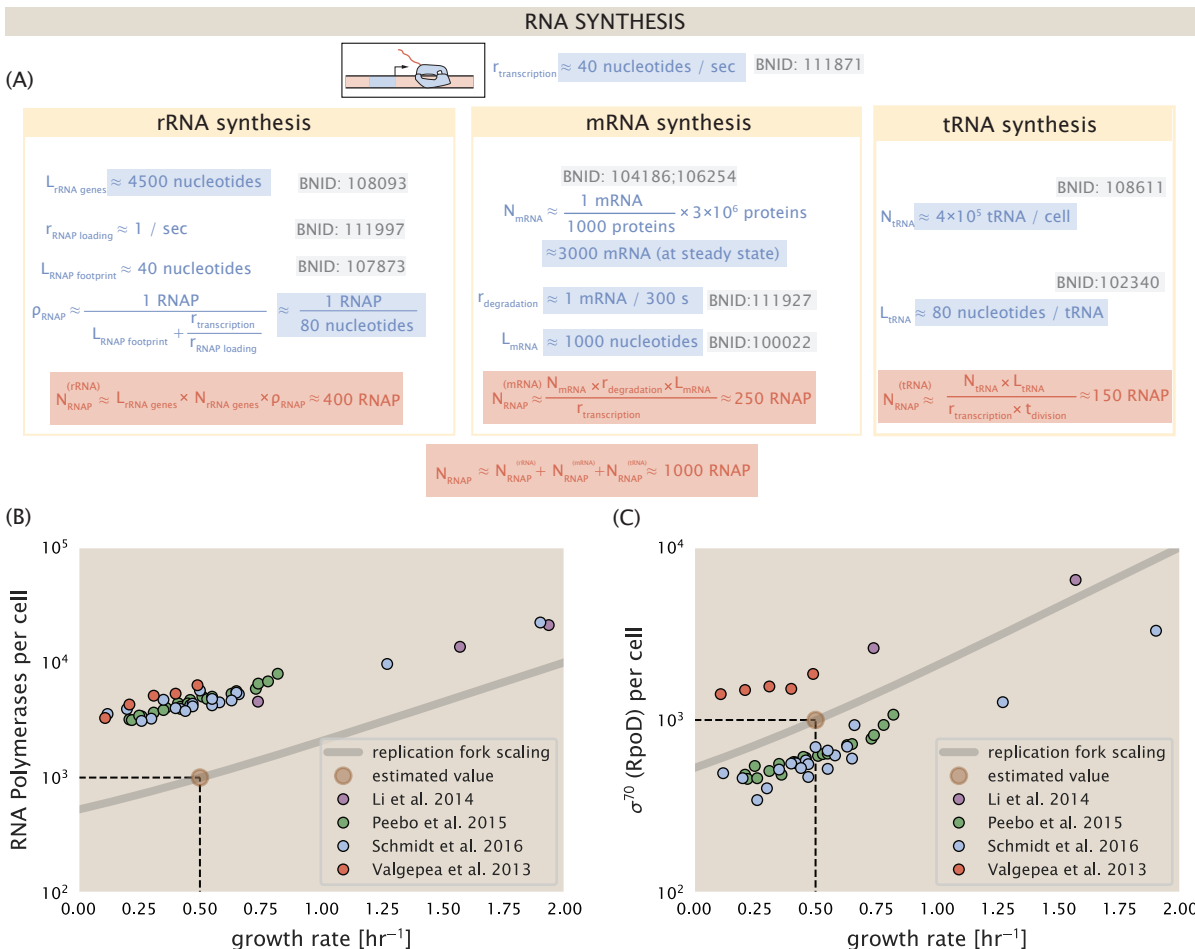


Figure 7. Estimation of the RNA polymerase demand and comparison with experimental data. (A) Estimations for the number of RNA polymerase needed to synthesize sufficient quantities of rRNA, mRNA, and tRNA from left to right, respectively. Bionumber Identifiers (BNIDs) are provided for key quantities used in the estimates. (B) The RNA polymerase core enzyme copy number as a function of growth rate. Colored points correspond to the average number RNA polymerase core enzymes that could be formed given a subunit stoichiometry of $[RpoA]_2[RpoC][RpoB]$. (C) The abundance of σ^{70} as a function of growth rate. Estimated value for the number of RNAP is shown in (B) and (C) as a translucent brown point at a growth rate of 0.5 hr^{-1} .

527 agreement with our estimate of the number of transcriptional complexes needed.

528 These estimates provide insight as to the observed magnitude of both RNA polymerase and
 529 the σ -70 factor. As we have done in the previous sections, and described in the supplemental
 530 information, we can generalize these estimates across a wide range of growth rates (grey line in
 531 **Figure 7(B)**). While there remains some disagreement in the magnitude of the copy number, this
 532 estimate appears to very adequately describe the growth rate dependence of these complexes.
 533 Furthermore, these findings illustrate that transcription cannot be the rate limiting step in bacterial
 534 division. **Figure 7(A)** reveals that the availability of RNA polymerase is not a limiting factor for cell
 535 division as the cell always has an apparent \sim 10-fold excess than needed. Furthermore, if more
 536 transcriptional activity was needed to satisfy the cellular requirements, more σ^{70} -factors could be
 537 expressed to utilize a larger fraction of the RNA polymerase pool.

538 Translation and ribosomal synthesis

539 Lastly, we turn our attention to the process of synthesizing new proteins, translation. This process
 540 stands as a good candidate for potentially limiting growth since the synthesis of new proteins relies
 541 on the generation of ribosomes, themselves proteinaceous molecules. As we will see in the coming
 542 sections of this work, this poses a "chicken-or-the-egg" problem where the synthesis of ribosomes
 543 requires ribosomes in the first place.

544 We will begin our exploration of protein translation in the same spirit as we have in previous
 545 sections – we will draw order-of-magnitude estimates based on our intuition and available literature,
 546 and then compare these estimates to the observed data. In doing so, we will estimate both the
 547 absolute number of ribosomes necessary for replication of the proteome as well as the synthesis
 548 of amino-acyl tRNAs. From there we consider the limitations on ribosomal synthesis in light of our
 549 estimates on both, the synthesis of ribosomal proteins, and our earlier results on rRNA synthesis.

550 tRNA synthetases

551 We begin by first estimating the number of tRNA ligases in *E. coli* needed to convert free amino-acids
 552 to polypeptide chains. At a modest growth rate of \approx 5000 s, *E. coli* has roughly 3×10^6 proteins per
 553 cell (BNID: 115702; *Milo et al. (2010)*). Assuming that the typical protein is on the order of \approx 300
 554 amino acids in length (BNID: 100017; *Milo et al. (2010)*), we can estimate that a total of $\approx 10^9$ amino
 555 acids are stitched together by peptide bonds.

556 How many tRNAs are needed to facilitate this remarkable number of amino acid delivery events
 557 to the translating ribosomes? It is important to note that tRNAs are recycled after they've passed
 558 through the ribosome and can be recharged with a new amino acid, ready for another round
 559 of peptide bond formation. While some *in vitro* data exists on the turnover of tRNA in *E. coli* for
 560 different amino acids, we can make a reasonable estimate by comparing the number of amino
 561 acids to be polymerized to cell division time. Using our stopwatch of 5000 s and 10^9 amino acids,
 562 we arrive at a requirement of $\approx 2 \times 10^5$ tRNA molecules. This estimate is in line with experimental
 563 measurements of $\approx 3 \times 10^5$ per cell (BNID: 108611, *Milo et al. (2010)*), suggesting we are on the
 564 right track.

565 There are many processes which go into synthesizing a tRNA and ligating it with the appropriate
 566 amino acids. As we covered in the previous section, there appear to be more than enough RNA
 567 polymerases per cell to synthesize the needed pool of tRNAs. Without considering the many ways
 568 in which amino acids can be scavenged or synthesized *de novo*, we can explore ligation as a
 569 potential rate limiting step. The enzymes which link the correct amino acid to the tRNA, known
 570 as tRNA synthetases or tRNA ligases, are incredible in their proofreading of substrates with the
 571 incorrect amino acid being ligated once out of every 10^4 to 10^5 times (BNID: 103469, *Milo et al.*
 572 *(2010)*). This is due in part to the consumption of energy as well as a multi-step pathway to ligation.
 573 While the rate at which tRNA is ligated is highly dependent on the identity of the amino acid, it
 574 is reasonable to state that the typical tRNA synthetase has charging rate of ≈ 20 AA per tRNA
 575 synthetase per second (BNID: 105279, *Milo et al. (2010)*).

576 Combining these estimates together, as shown schematically in **Figure 8(A)**, yields an estimate
 577 of $\approx 10^4$ tRNA synthetases per cell with a division time of 5000 s. This point estimate is in very close
 578 agreement with the observed number of synthetases (the sum of all 20 tRNA synthetases in *E. coli*).
 579 This estimation strategy seems to adequately describe the observed growth rate dependence of
 580 the tRNA synthetase copy number (shown as the grey line in **Figure 8(B)**), suggesting that the copy
 581 number scales with the cell volume.

582 In total, the estimated and observed $\approx 10^4$ tRNA synthetases occupy only a meager fraction of
 583 the total cell proteome, around 0.5% by abundance. It is reasonable to assume that if tRNA charging
 584 was a rate limiting process, cells would be able to increase their growth rate by devoting more
 585 cellular resources to making more tRNA synthases. As the synthesis of tRNAs and the corresponding
 586 charging can be highly parallelized, we can argue that tRNA charging is not a rate limiting step in
 587 cell division, at least for the growth conditions explored in this work.

588 Protein synthesis

589 With the number of tRNA synthetases accounted for, we now consider the abundance of the protein
 590 synthesis machines themselves, ribosomes. Ribosomes are enormous protein/rRNA complexes
 591 that facilitate the peptide bond formation between amino acids in the correct sequence as defined
 592 by the coding mRNA. Before we examine the synthesis of the ribosome proteins and the limits that
 593 may place on the observed bacterial growth rates, let's consider replication of the cellular proteome.

594 As described in the previous section, *E. coli* consists of $\approx 3 \times 10^6$ proteins at a growth rate of \approx
 595 5000 s. If we again assume that each protein is composed of ≈ 300 amino acids and each amino
 596 acid is linked together by one peptide bond, we arrive at an estimate that the cellular proteome
 597 consists of $\approx 10^{10}$ peptide bonds. While the rate at which ribosomes translates is well known to
 598 have a growth rate dependence *Dai et al. (2018)* and is a topic which we discuss in detail in the
 599 coming sections. However, for the purposes of our order-of-magnitude estimate, we can make the
 600 approximation that translation occurs at a rate of ≈ 15 amino acids per second per ribosome (BNID:
 601 100233, *Milo et al. (2010)*). Under this approximation and assuming a division time of 5000 s, we
 602 can arrive at an estimate of $\approx 10^4$ ribosomes are needed to replicate the cellular proteome, shown
 603 in **Figure 8(B)**. This point estimate, while glossing over important details such as chromosome
 604 copy number and growth-rate dependent translation rates, proves to be notably accurate when
 605 compared to the experimental observations (**Figure 8(B)**).

606 Translation as a growth-rate limiting step

607 Thus far, the general back-of-the-envelope estimates have been reasonably successful in explaining
 608 what sets the scale of absolute protein copy number. A recurring theme that has arisen is the ability
 609 of cells to parallelize their biosynthesis tasks. For example, while DNA replication speed-limit is ≈ 40
 610 minutes to replicate a genome, cells can divide faster than this by initiating more than one round of
 611 replication per doubling. However, as we will see, parallelization is not possible when it comes to
 612 the translation of ribosomal proteins (**Figure 9(A)**). Thus, it is plausible that translation may be a key
 613 factor in determining the cellular growth rate.

614 To gain some intuition into how translation can set the speed of bacterial growth, we again
 615 consider the total number of peptide bonds that must be synthesized, which we denote as N_{AA} .
 616 Noting that cells grow exponentially in time (*Godin et al., 2010*), we can compute the number of
 617 amino acids to be polymerized as

$$N_{AA} \lambda = r_t R, \quad (1)$$

618 where λ is the cell growth rate in s^{-1} , r_t is the maximum translation rate in $AA \cdot s^{-1}$, and R is the
 619 average ribosome copy number per cell. Knowing the number of peptide bonds to be formed
 620 permits us to compute the translation-limited growth rate as

$$\lambda_{\text{translation-limited}} = \frac{r_t R}{N_{AA}}. \quad (2)$$

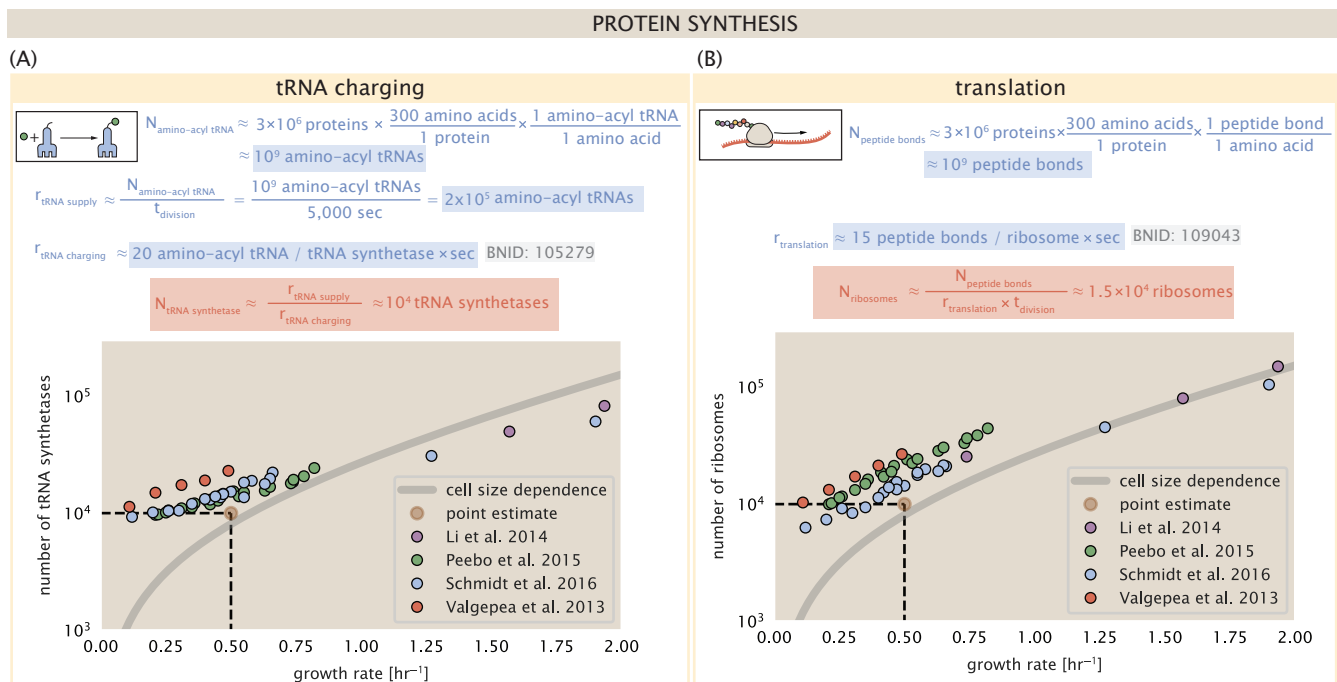


Figure 8. Estimation of the required tRNA synthetases and ribosomes. (A) Estimation for the number of tRNA synthetases that will supply the required amino acid demand. The sum of all tRNA synthetases copy numbers are plotted as a function of growth rate ([ArgS], [CysS], [GlnS], [Glx], [IleS], [LeuS], [ValS], [AlaS]₂, [AsnS]₂, [AspS]₂, [TyrS]₂, [TrpS]₂, [ThrS]₂, [SerS]₂, [ProS]₂, [PheS]₂[PheT]₂, [MetG]₂, [IysS]₂, [HisS]₂, [GlyS]₂[GlyQ]₂). (B) Estimation of the number of ribosomes required to synthesize 10⁹ peptide bonds with an elongation rate of 15 peptide bonds per second. The average abundance of ribosomes is plotted as a function of growth rate. Our estimated values are shown for a growth rate of 0.5 hr⁻¹. Grey lines correspond to the estimated complex abundance calculated at different growth rates. See Supplemental Information XX for a more detailed description of this calculation.

621 Alternatively, since N_{AA} is related to the total protein mass through the molecular weight of
 622 each protein, we can also consider the growth rate in terms of the fraction of the total proteome
 623 mass that is dedicated to ribosomal protein mass. By making the approximation that an average
 624 amino acid has a molecular weight of 110 Da (BNID: 104877, *Milo et al. (2010)*), we can approximate
 625 $R/N_{AA} \approx \Phi_R/L_R$, where Φ_R is the ribosomal mass fraction and L_R is the total length in amino acids
 626 that make up a ribosome. The translation-limited growth rate can then be written in the form

$$\lambda_{\text{translation-limited}} \approx \frac{r_t}{L_R} \Phi_R. \quad (3)$$

627 This is plotted as a function of ribosomal fraction Φ_R in **Figure 9(B)**, where we take $L_R \approx 7500$ AA,
 628 corresponding to the length in amino acids for all ribosomal subunits of the 50S and 30S complex
 629 (BNID: 101175, *(Milo et al., 2010)*).

630 The growth rate defined by **Equation 3** reflects mass-balance under steady-state growth and
 631 has long provided a rationalization of the apparent linear increase in *E. coli*'s ribosomal content
 632 as a function of growth rate (*Maaløe, 1979; Scott et al., 2010*). We note that there is a maximum
 633 growth rate of $\lambda \approx 8 \text{ hr}^{-1}$, or a doubling time just under 6 minutes (**Figure 9(B)**, dashed line). This
 634 represents an inherent speed limit due to the need for the cell to double its entire ribosomal mass.
 635 Interestingly, this limit is independent of the absolute number of ribosomes and is simply given by
 636 the time to translate an entire ribosome, L_R/r_t . As shown in **Figure 9(A)**, we can reconcile this with
 637 the observation that in order to double the average number of ribosomes, each ribosome must
 638 produce a second ribosome and cannot be parallelized.

639 Earlier, we considered rRNA synthesis (see Section **RNA Synthesis**), finding that, when the rRNA
 640 operons are maximally loaded with RNA polymerase, the cell can produce ≈ 1 functional rRNA
 641 unit per second per operon. In **Figure 9(C)**, we show the maximum number of ribosomes that
 642 could be made as a function of growth rate given this rRNA production rule-of-thumb. While each
 643 *E. coli* genome has 7 copies of the rRNA operon (BNID: 107866, *Milo et al. (2010)*), parallelization
 644 of DNA synthesis by firing multiple rounds of replication at a time can drastically increase the effective
 645 number of rRNA operons. The blue curve in ??, we assume that the effective number of rRNA
 646 operons increases in proportion to the number of origins of replication ($\# \text{ ori}$) (solid blue line;
 647 with the calculation of ($\# \text{ ori}$) described in the next section). Although we expect this value to
 648 drastically overestimate rRNA abundance at slower growth rates ($\lambda < 0.5 \text{ hr}^{-1}$), it provides a useful
 649 reference when considered along with the proteomic measurements that are also plotted. For
 650 growth rates above about 1 hr^{-1} , we find that cells will need to transcribe rRNA near their maximal
 651 rate. The dashed blue curve in **Figure 9(C)** shows the maximal number of functional rRNA units
 652 that could be synthesized from a single genome (ignoring the chromosome replication speed limit
 653 of ≈ 40 minutes per genome). The convergence between the maximum rRNA production with
 654 parallelization and the experimentally measured ribosome copy number (points in **Figure 9(C)**),
 655 as well as the observation cells are rarely reported to grow faster than 2 hr^{-1} [GC: Can we find a
 656 citation for this?], suggests rRNA synthesis represents the rate limiting step in cell division for this
 657 strain of *E. coli*.

658 Relationship between cell size and growth rate.

659 With the observation that ribosomes set an inherent upper limit on growth rate, through both
 660 rRNA synthesis and the additional dependence on ribosomal fraction, it is also plausible that
 661 ribosomes may play a more dominant role in setting growth rate across other growth conditions.
 662 With a rich proteomic data set across a wide array of conditions, and in light of a number of recent
 663 experimental observations, we find that cells also appear to tune their ribosomal abundance as a
 664 means to maximize growth even in poor nutrient conditions. This has important consequences on
 665 the relationship with cell size and maintenance of steady-state growth. In the coming section and
 666 the remainder of the text, we consider these further beginning with cell size.

667 The relationship between cell size and growth rate has long been of interest in the study of
 668 bacterial physiology, particularly following the now six decade-old observation that cell volume

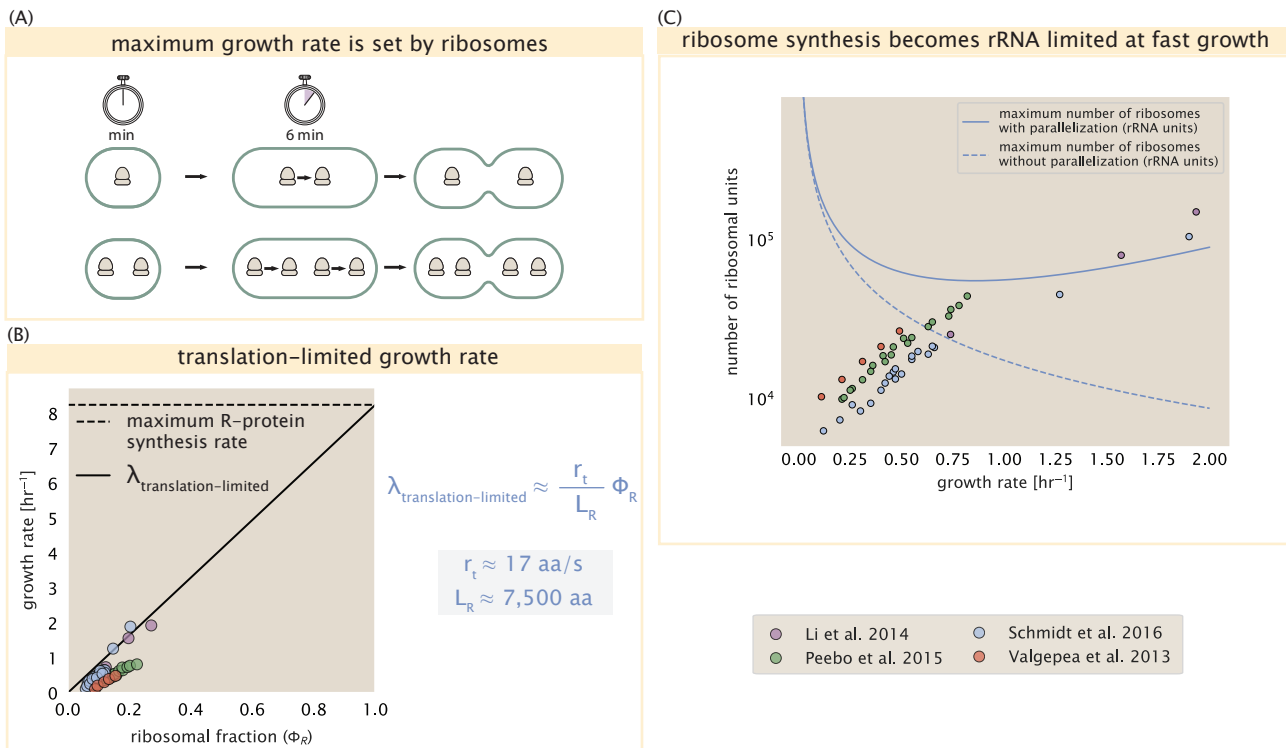


Figure 9. Translation-limited growth rate. (A) Here we consider the translation-limited growth as a function of ribosomal fraction. By mass balance, the time required to double the entire proteome (N_{AA} / r_t) sets the translation-limited growth rate, $\lambda_{\text{translation-limited}}$. Here N_{aa} is effectively the number of peptide bonds that must be translated, r_t is the translation elongation rate, and R is the number of ribosomes. This can also be re-written in terms of the ribosomal mass fraction $\Phi_R = m_R / m_{\text{protein}}$, where m_R is the total ribosomal mass and m_{protein} is the mass of all proteins in the cell. L_R refers to the summed length of the ribosome in amino acids. $\lambda_{\text{translation-limited}}$ is plotted as a function of Φ_R (solid line). (B) The dashed line in part (A) identifies a maximum growth rate that is set by the ribosome. Specifically, this growth rate corresponds to the time required to translate an entire ribosome, L_R / r_t . This is a result that is independent of the number of ribosomes in the cell as shown schematically here. (C) Maximum number of rRNA units that can be synthesized as a function of growth rate. Solid curve corresponds to the rRNA copy number calculated by multiplying the number of rRNA operons by the estimated number of (# ori) at each growth rate. The quantity (# ori) was calculated using Equation 4 and the measurements from Si et al. (2017) that are plotted in Figure 10(A). Dashed line show that maximal number of functional rRNA units produced from a single chromosome without parallelization.

669 appears to increase exponentially with growth rate; known as Schaechter's growth law (*Schaechter et al., 1958; Taheri-Araghi et al., 2015*). Wild-type *E. coli* growing at relatively fast growth rates
 670 exhibit a remarkably constant cell cycle time t_{cyc} (referring to the C and D periods of DNA replication
 671 and cell division, respectively), as shown in **Figure 10(A)** for the data reproduced from (*Si et al., 2017*). With a constant cell cycle time, the exponential scaling in size has long been considered
 672 a direct consequence of cells initiating replication at a constant volume per origin. However, the
 673 particular mechanism that governs this relationship, and even the question of whether the change
 674 in average cell size is truly exponential have remained under debate (*Si et al., 2017; Harris and Theriot, 2018*).
 675

676 Since protein accounts for more than half of cellular dry mass (BNID: 104954, *Milo et al. (2010); Bremer and Dennis (2008); Basan et al. (2015)*, cell size will vary in proportion to how much protein
 677 is synthesized over the cell cycle. Through our estimates in the sections on the central dogma, it is
 678 apparent that the processes of transcription (i.e. synthesis of mRNA) and translation are unlikely
 679 limiting steps in doubling the cell mass. In both cases, there is an overabundance of the requisite
 680 protein complexes (DNA and RNA polymerase, respectively) and there are mechanisms by which
 681 these synthesis processes can be parallelized. Therefore, the total protein mass is determined by
 682 $r_t \times R$ and the doubling time τ . The relationship between cell size and growth rate, however, will
 683 depend only on how the cell scales its ribosomal fraction Φ_R , as highlighted by **Equation 3**.
 684

685 Ribosomal abundance defines exponential scaling between cell size and growth rate
 686 A naïve strategy to increase growth rate given the constraint prescribed by **Equation 3**, would be to
 687 simply generate more ribosomes. In reality, large swaths of the proteome increases in absolute
 688 abundance at faster growth (Supplemental Figure X). Substantial empirical evidence has revealed a
 689 linear scaling between cell size (volume) and the number of chromosomal origins of replication,
 690 $\langle \# \text{ ori} \rangle$, which is robust to a remarkable array of perturbations (*Si et al., 2017*). The number of
 691 origins $\langle \# \text{ ori} \rangle$ is determined by how often replication must be initiated per cell doubling to maintain
 692 steady-state growth. This quantity can be approximately quantified via
 693

$$\langle \# \text{ ori} \rangle \approx 2^{\tau_{cyc}/\tau}, \quad (4)$$

694 where τ is the doubling time. In **Figure 10(A)**, we show the measurements of *Si et al. (2017)* for
 695 wild-type *E. coli* cells in nutrient-limit growth regimes. Using this data, we estimated $\langle \# \text{ ori} \rangle$ for each
 696 condition in the amalgamated proteomic datasets. With rRNA otherwise becoming rate limited at
 697 fast growth, this strategy allows for a roughly linear increase in ribosomes copy number with $\langle \# \text{ ori} \rangle$
 698 as shown in **Figure 10(B)** for the proteomic data.
 699

700 It is notable that in *E. coli*, the majority of ribosomal proteins and rRNA operons are found
 701 closer to the origin of replication. Since multiple rounds of DNA initiation will effectively skew gene
 702 dosage in favor of genes near the origin (*Scholz et al., 2019*), it suggests that an increase in $\langle \# \text{ ori} \rangle$
 703 is a means to skew the ribosomal fraction of the proteome, Φ_R . In **Figure 10(D)** we show that this
 704 skew in gene dosage is reflected in the composition of the proteome via a running boxcar average
 705 (500 kbp window) of protein copy number as a function of each gene's transcriptional start site
 706 (**Figure 10(D)**). While the protein copy numbers of individual proteins can vary substantially across
 707 the entire chromosome, we nonetheless observe a bias in expression across the chromosome
 708 under fast growth conditions (dark blue lines) relative to slow growth (yellow lines). The dramatic
 709 change in protein copy number near the origin is largely due to the increase in ribosomal protein
 710 expression. This trend is in contrast to slower growth conditions (yellow) where the average copy
 711 number is much more uniform across the length of the chromosome.

712 This result provides important evidence that although total protein content scales with $\langle \# \text{ ori} \rangle$, it
 713 is also the bias in gene dosage for genes closer to the origin that change the proteomic composition
 714 and allows an increase in the ribosomal fraction Φ_R at fast growth. For *E. coli*, we can then view
 715 the increase in ribosomal fraction Φ_R (and therefore, λ) as requiring a geometric increase in total
 716 protein abundance that is proportional to $\langle \# \text{ ori} \rangle$. This leads to an exponential increase in total

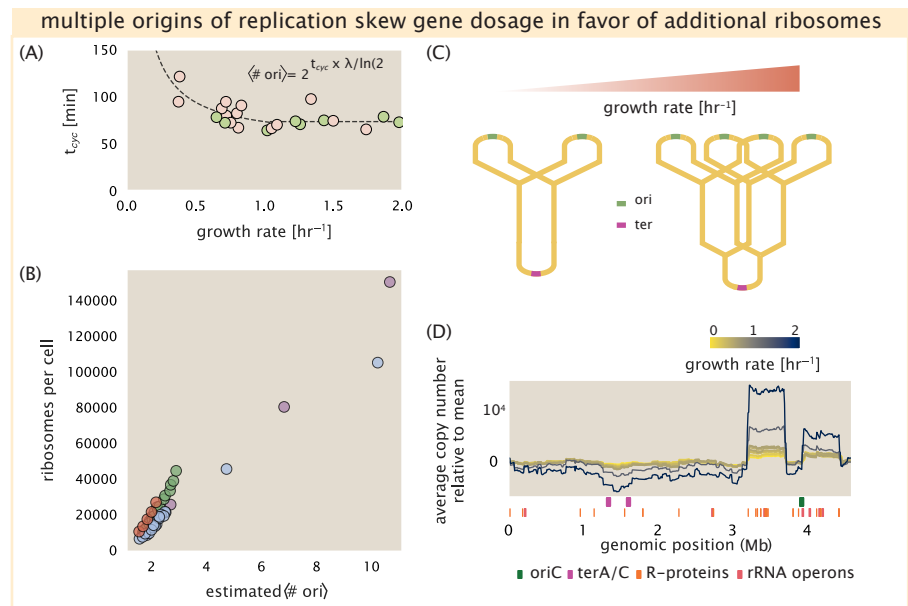


Figure 10. Multiple replication forks skew gene dosage and ribosomal content. (A) Experimental data from Si *et al.* (2017). Dashed line shows fit to the data, which were used to estimate $\langle \# \text{ori} \rangle$. t_{cyc} was assumed to vary in proportion to τ for doubling times great than 40 minutes, and then reach a minimum value of [fill in] minutes below this (see Supplemental Appendix X for additional details). Red data points correspond to measurements in strain MG1655, while light green points are for strain NCM3722. (B) Plot of the ribosome copy number estimated from the proteomic data against the estimated $\langle \# \text{ori} \rangle$ [NB: change to total protein abundance?]. (C) Schematic shows the expected increase in replication forks (or number of ori regions) as *E. coli* cells grow faster. (D) A running boxcar average of protein copy number is calculated for each each growth condition considered by (Schmidt *et al.*, 2016). A 0.5 Mb averaging window was used. Protein copy numbers are reported relative to their condition-specific means in order to center all data sets.

717 protein mass (and cell size) as long as all ribosomes R are actively translating protein during cell
718 doubling.

719 Growth in poor nutrient conditions.

720 While the above results suggest that it is the need to increase the number of ribosomes that sets
721 an exponential scaling in cell size, this relationship is likely to falter at slow growth rates (below
722 $\lambda \approx 0.5 \text{ hr}^{-1}$). In this regime, ribosome copy number R no longer reflects the cell's protein synthesis
723 capacity [GC: Not sure I understand the previous sentence. It's not R , but $r, R\tau$ that's the translational
724 capacity, no?]. While cells appear to maintain a scaling of R with $\langle \# \text{ori} \rangle$ (Figure 10(A)) even at slow
725 growth rates (reaching a minimum ribosomal mass fraction of $\Phi_R \approx 0.06$), additional regulatory
726 control through the small-molecule alarmones such as guanosine pentaphosphate [(p)ppGpp]
727 reduces the fraction of actively translating ribosomes at slow growth (Dai *et al.*, 2016; Bosdriesz
728 *et al.*, 2015; Zhu and Dai, 2019)[GC: "yielding a translational capacity below $r, R\tau$."]. In this section
729 we consider the consequence of having excess ribosomes on maintaining steady-state growth in
730 poor nutrient conditions.

731 How do cells regulate protein synthesis when amino acids can be limiting, meaning consumption
732 exceeds the rate of synthesis? At slow growth rates, this imbalance would occur if the entire
733 ribosomal pool were actively translating (Figure 11). Without additional regulatory control, this
734 would prevent continuous growth, and indeed for (p)ppGpp null strains, cells only grow in minimal
735 media if additional amino acid supplements are present. In contrast, wild-type *E. coli* maintain a
736 relatively high elongation rate even in stationary phase ($\approx 8 \text{ AA/s}$, (Dai *et al.*, 2016, 2018)).

737 Mitigation of translation activity helps maintain homeostasis in poor nutrient conditions
738 To better understand how regulation of ribosomes influence growth rate in slow growth regimes,
739 we consider a coarse-grained model that relates elongation rate to a limiting supply of amino

740 acids, which for simplicity we treat as a single, effective rate-limiting species $[AA]_{eff}$. Under such a
 741 scenario, the elongation rate r_t can be described as depending on the maximum elongation rate
 742 ($r_t^{max} \approx 17.1$ aa/s, (Dai et al., 2016, 2018)), an effective binding constant K_D between the pool of
 743 amino acids and their amino-acyl tRNAs, and the limiting amino acid concentration $[AA]_{eff}$,

$$r_t = r_t^{max} \cdot \frac{1}{1 + K_D/[AA]_{eff}}. \quad (5)$$

744 For cells growing in minimal medium supplemented with glucose, the amino acid concentration is
 745 of order 100 mM (BNID: 110093, (Milo et al., 2010; Bennett et al., 2009)). To estimate K_D , we note
 746 that for a growth rate of about 0.6 hr⁻¹ Dai et al. (2016) measured an elongation rate of about 12.5
 747 AA·s⁻¹, yielding $K_D \approx 40$ mM. The maintenance of this amino acid pool $[AA]_{eff}$ will depend on the
 748 difference between the synthesis/supply rate of amino acids r_{AA} and consumption by ribosomes
 749 $r_t \times R \times f_a$, where we use f_a to account for the possible reduction of actively translating ribosomes
 750 (see Supplemental Appendix XX for further details on this model).

751 In Figure 11(B), we show the relationship between the growth rate and elongation rate as a
 752 function of the number of actively translating ribosomes. Here, growth rate is now determined by
 753 the active ribosomal fraction via

$$\lambda_{\text{translation-limited}} \approx \frac{r_t}{L_R} \Phi_R f_a. \quad (6)$$

754 If we consider constant values of amino acid synthesis rate r_{AA} (dashed lines) to reflect the available
 755 parameter space for a specific growth condition, the fastest growth rates result from maximization
 756 of the fraction of actively translating ribosomes. When we consider the experimental measurements
 757 from Dai et al. (2018) (yellow circles), reflecting growth in different nutrient conditions, we see that
 758 although $R \times f_a$ is reduced in poorer nutrient conditions, it is reduced in a manner such that $[AA]_{eff}$
 759 is relatively constant. Given our estimate $K_D \approx 40$ mM, we would only expect a decrease from 100
 760 mM to about 35 mM in the slowest growth conditions. While experimental data is scarce, amino
 761 acid concentrations only decrease to about 60 mM for cells grown in minimal media supplemented
 762 with acetate ($\lambda \approx 0.3$ hr⁻¹ in our proteomic data) (Bennett et al., 2009) is qualitatively consistent
 763 with our expectations [GC: Report a value from the bennet paper here?]. One explanation for the
 764 experimental data is that the active fraction of the ribosome pool is regulated in order to maintain
 765 a sufficient supply of amino acids for growth. Any further increase in $R \times f_a$ at constant r_{AA} would
 766 otherwise be associated with an additional drop in cellular amino acid concentration.

767 *E. coli* maximizes its steady-state growth rate by tuning both ribosomal content and
 768 translation activity.

769 Using the active fraction f_a measurements across a broad range of nutrient-limited growth conditions
 770 from the work of Dai et al. (2016), we furthermore estimated the active fraction of ribosomal
 771 protein across the collated proteomic datasets (Figure 11(C)). Importantly, we note that across all
 772 growth conditions considered cells appear to maintain a growth rate consistent with Equation 3
 773 with an elongation rate of $r_t \approx 17.1$ aa/s. While somewhat counter intuitive, given that ribosomes
 774 translate at almost half this rate in the poorest of growth conditions, steady-state growth rates can
 775 be achieved over such a broad range of conditions because cells have evolved a means to tune
 776 $r_t \times R \times f_a$.

777 It has recently been shown that growth in a (p)ppGpp null strain abolishes both the scaling
 778 in cell size and the $\langle \# \text{ori} \rangle / \langle \# \text{ter} \rangle$ ratio [GC: Note here we return to a discussion of ori/ter ratio,
 779 but I think that has been cut earlier. Can we just say the scaling between cell size and ori?].
 780 Instead, cells exhibited a high $\langle \# \text{ori} \rangle / \langle \# \text{ter} \rangle$ closer to 4 and cell size more consistent with a fast
 781 growth state where (p)ppGpp levels are low (Fernández-Coll et al., 2020) and ribosomal fraction is
 782 high (Zhu and Dai, 2019). This raises the possibility that the action of (p)ppGpp is also mediating
 783 growth control and size scaling over this entire range of growth conditions. Specifically, as nutrient
 784 conditions worsen, (p)ppGpp helps decrease multiple rounds of DNA replication per cell doubling

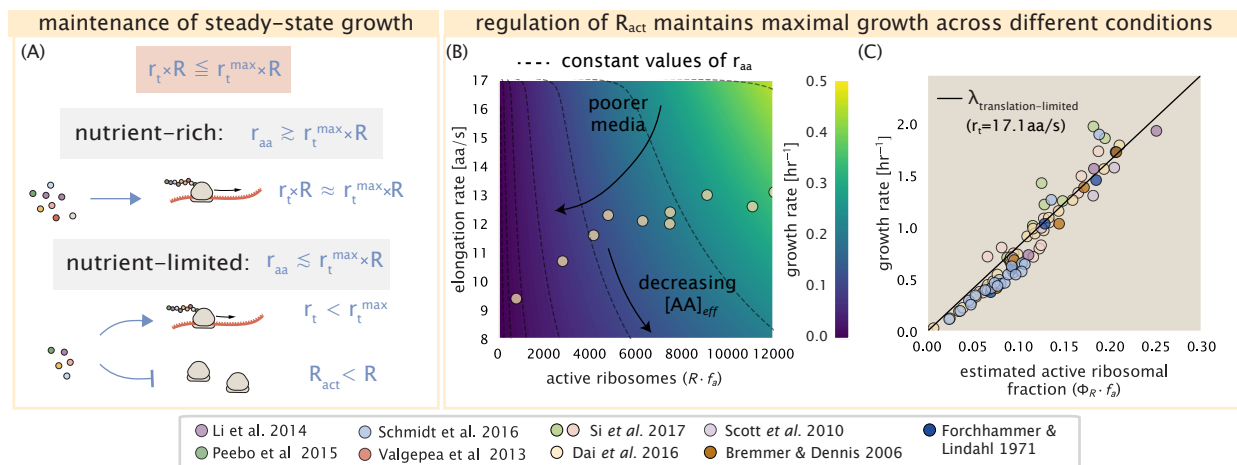


Figure 11. *E. coli* must regulate ribosomal activity in limiting nutrient conditions. (A) Schematic showing translation-specific requirements for maintenance of steady-state growth. In a nutrient rich environment, amino acid supply r_{aa} is sufficiently in excess of the demand by ribosomes translating at their maximal rate. In poorer nutrient conditions, reduced amino acid supply r_{aa} will decrease the rate of elongation. In a regime where r_{aa} is less than $r_t R$, the number of actively translating ribosomes will need to be reduced in order to maintain steady-state growth. (B) Translation elongation rate is plotted as a function of the number of actively translating ribosomes Rf_a . Dashed lines correspond to a range of amino acid synthesis rates r_{aa} , from 10^3 to 10^6 . Growth rates are calculated according to Equation 1, assuming a constant ribosomal fraction of 8 percent. See appendix XX for additional details. (C) Experimental data from (Dai et al., 2016) are used to estimate the fraction of actively translating ribosomes. The solid line represents the translation-limited growth rate for ribosomes elongating at 17.1 AA/s.

which effectively decreases both R and the total cell size *and* in sufficiently poor growth conditions mitigates translation activity according to nutrient availability.

787 References

- 788 **Abelson HT**, Johnson LF, Penman S, Green H. Changes in RNA in Relation to Growth of the Fibroblast: II.
 789 The Lifetime of mRNA, rRNA, and tRNA in Resting and Growing Cells. *Cell*. 1974 Apr; 1(4):161–165. doi:
 790 10.1016/0092-8674(74)90107-X.
- 791 **Aidenberg G**, Towbin BD, Rothschild D, Dekel E, Bren A, Alon U. Hierarchy of Non-Glucose Sugars in *Escherichia*
 792 *coli*. *BMC Systems Biology*. 2014 Dec; 8(1):133. doi: 10.1186/s12918-014-0133-z.
- 793 **Antonenko YN**, Pohl P, Denisov GA. Permeation of Ammonia across Bilayer Lipid Membranes Studied by
 794 Ammonium Ion Selective Microelectrodes. *Biophysical Journal*. 1997 May; 72(5):2187–2195.
- 795 **Ashburner M**, Ball CA, Blake JA, Botstein D, Butler H, Cherry JM, Davis AP, Dolinski K, Dwight SS, Eppig JT, Harris
 796 MA, Hill DP, Issel-Tarver L, Kasarskis A, Lewis S, Matese JC, Richardson JE, Ringwald M, Rubin GM, Sherlock G.
 797 Gene Ontology: tool for the unification of biology. *Nature Genetics*. 2000 May; 25(1):25–29.
- 798 **Ason B**, Bertram JG, Hingorani MM, Beechem JM, O'Donnell M, Goodman MF, Bloom LB. A Model for *Escherichia*
 799 *coli* DNA Polymerase III Holoenzyme Assembly at Primer/Template Ends: DNA Triggers A Change In Binding
 800 Specificity of the γ Complex Clamp Loader. *Journal of Biological Chemistry*. 2000 Jan; 275(4):3006–3015. doi:
 801 10.1074/jbc.275.4.3006.
- 802 **Assentoft M**, Kaptan S, Schneider HP, Deitmer JW, de Groot BL, MacAulay N. Aquaporin 4 as a NH₃ Channel.
 803 *Journal of Biological Chemistry*. 2016 Sep; 291(36):19184–19195. doi: 10.1074/jbc.M116.740217.
- 804 **Basan M**, Zhu M, Dai X, Warren M, Sévin D, Wang YP, Hwa T. Inflating bacterial cells by increased protein
 805 synthesis. *Molecular Systems Biology*. 2015 Oct; 11(10):836.
- 806 **Bauer S**, Ziv E. Dense Growth of Aerobic Bacteria in a Bench-Scale Fermentor. *Biotechnology and Bioengineering*.
 807 1976; 18(1):81–94. doi: 10.1002/bit.260180107, eprint:
 808 <https://onlinelibrary.wiley.com/doi/pdf/10.1002/bit.260180107>.
- 809 **Belliveau NM**, Barnes SL, Ireland WT, Jones DL, Sweredoski MJ, Moradian A, Hess S, Kinney JB, Phillips R. Systematic Approach for Dissecting the Molecular Mechanisms of Transcriptional Regulation in Bacteria. *Proceedings of the National Academy of Sciences*. 2018 May; 115(21):E4796–E4805. doi: 10.1073/pnas.1722055115.
- 812 **Bennett BD**, Kimball EH, Gao M, Osterhout R, Van Dien SJ, Rabinowitz JD. Absolute metabolite concentrations
 813 and implied enzyme active site occupancy in *Escherichia coli*. *Nature Chemical Biology*. 2009 Aug; 5(8):593–599.
- 814 **Birnbaum LS**, Kaplan S. Localization of a Portion of the Ribosomal RNA Genes in *Escherichia coli*. *Proceedings of the National Academy of Sciences*. 1971 May; 68(5):925–929. doi: 10.1073/pnas.68.5.925.
- 816 **Booth IR**, Mitchell WJ, Hamilton WA. Quantitative Analysis of Proton-Linked Transport Systems. The Lactose
 817 Permease of *Escherichia coli*. *Biochemical Journal*. 1979 Sep; 182(3):687–696.
- 818 **Bosdriesz E**, Molenaar D, Teusink B, Bruggeman FJ. How fast-growing bacteria robustly tune their ribosome
 819 concentration to approximate growth-rate maximization. *The FEBS Journal*. 2015 May; 282(10):2029–2044.
- 820 **Bremer H**, Dennis PP. Modulation of Chemical Composition and Other Parameters of the Cell at Different
 821 Exponential Growth Rates. *EcoSal Plus*. 2008 Oct; 3(1).
- 822 **Browning DF**, Busby SJW. Local and global regulation of transcription initiation in bacteria. *Nature Reviews Microbiology*. 2016 Aug; 14(10):638–650.
- 824 **Cox GB**, Newton NA, Gibson F, Snoswell AM, Hamilton JA. The Function of Ubiquinone in *Escherichia coli*.
 825 *Biochemical Journal*. 1970 Apr; 117(3):551–562. doi: 10.1042/bj1170551.
- 826 **Dai X**, Zhu M, Warren M, Balakrishnan R, Okano H, Williamson JR, Fredrick K, Hwa T. Slowdown of Translational
 827 Elongation in *Escherichia coli* under Hyperosmotic Stress. - PubMed - NCBI. *mBio*. 2018 Feb; 9(1):281.
- 828 **Dai X**, Zhu M, Warren M, Balakrishnan R, Patsalo V, Okano H, Williamson JR, Fredrick K, Wang YP, Hwa T. Reduction
 829 of translating ribosomes enables *Escherichia coli* to maintain elongation rates during slow growth. *Nature Microbiology*. 2016 Dec; 2(2):16231.
- 831 **Escalante A**, Salinas Cervantes A, Gosset G, Bolívar F. Current Knowledge of the *Escherichia coli* Phosphoenolpyruvate–Carbohydrate Phosphotransferase System: Peculiarities of Regulation and Impact on Growth and Product Formation. *Applied Microbiology and Biotechnology*. 2012 Jun; 94(6):1483–1494. doi: 10.1007/s00253-012-4101-5.

- 835 **Feist AM**, Henry CS, Reed JL, Krummenacker M, Joyce AR, Karp PD, Broadbelt LJ, Hatzimanikatis V, Palsson BØ. A
836 Genome-Scale Metabolic Reconstruction for *Escherichia coli* K-12 MG1655 That Accounts for 1260 ORFs and
837 Thermodynamic Information. *Molecular Systems Biology*. 2007 Jan; 3(1):121. doi: 10.1038/msb4100155.
- 838 **Fernández-Coll L**, Maciąg-Dorszynska M, Tailor K, Vadia S, Levin PA, Szalewska-Palasz A, Cashel M, Dunny GM.
839 The Absence of (p)ppGpp Renders Initiation of *Escherichia coli* Chromosomal DNA Synthesis Independent of
840 Growth Rates. *mBio*. 2020 Apr; 11(2):45.
- 841 **Fijalkowska IJ**, Schaaper RM, Jonczyk P. DNA Replication Fidelity in *Escherichia coli*: A Multi-DNA Polymerase
842 Affair. *FEMS Microbiology Reviews*. 2012 Nov; 36(6):1105–1121. doi: 10.1111/j.1574-6976.2012.00338.x.
- 843 **Finkelstein IJ**, Greene EC. Molecular Traffic Jams on DNA. *Annual Review of Biophysics*. 2013 May; 42(1):241–263.
- 844 **Gama-Castro S**, Salgado H, Santos-Zavaleta A, Ledezma-Tejeida D, Muñiz-Rascado L, García-Sotelo JS, Alquicira-
845 Hernández K, Martínez-Flores I, Pannier L, Castro-Mondragón JA, Medina-Rivera A, Solano-Lira H, Bonavides-
846 Martínez C, Pérez-Rueda E, Alquicira-Hernández S, Porrón-Sotelo L, López-Fuentes A, Hernández-Koutoucheva
847 A, Moral-Chávez VD, Rinaldi F, et al. RegulonDB Version 9.0: High-Level Integration of Gene Regulation,
848 Coexpression, Motif Clustering and Beyond. *Nucleic Acids Research*. 2016 Jan; 44(D1):D133–D143. doi:
849 10.1093/nar/gkv1156.
- 850 **Ge J**, Yu G, Ator MA, Stubbe J. Pre-Steady-State and Steady-State Kinetic Analysis of *E. coli* Class I Ribonucleotide
851 Reductase. *Biochemistry*. 2003 Sep; 42(34):10071–10083. doi: 10.1021/bi034374r.
- 852 **Godin M**, Delgado FF, Son S, Grover WH, Bryan AK, Tzur A, Jorgensen P, Payer K, Grossman AD, Kirschner
853 MW, Manalis SR. Using buoyant mass to measure the growth of single cells. *Nature Methods*. 2010 Apr;
854 7(5):387–390.
- 855 **Goldman SR**, Nair NU, Wells CD, Nickels BE, Hochschild A. The Primary σ Factor in *Escherichia coli* Can Access the
856 Transcription Elongation Complex from Solution *in Vivo*. *eLife*. 2015 Sep; 4:e10514. doi: 10.7554/eLife.10514.
- 857 **Harris LK**, Theriot JA. Surface Area to Volume Ratio: A Natural Variable for Bacterial Morphogenesis. *Trends in
858 microbiology*. 2018 Oct; 26(10):815–832.
- 859 **Harris RM**, Webb DC, Howitt SM, Cox GB. Characterization of PitA and PitB from *Escherichia coli*. *Journal of
860 Bacteriology*. 2001 Sep; 183(17):5008–5014. doi: 10.1128/JB.183.17.5008-5014.2001.
- 861 **van Heeswijk WC**, Westerhoff HV, Boogerd FC. Nitrogen Assimilation in *Escherichia coli*: Putting Molecular
862 Data into a Systems Perspective. *Microbiology and Molecular Biology Reviews*. 2013 Dec; 77(4):628–695. doi:
863 10.1128/MMBR.00025-13.
- 864 **Heldal M**, Norland S, Tumyr O. X-Ray Microanalytic Method for Measurement of Dry Matter and Elemental
865 Content of Individual Bacteria. *Applied and Environmental Microbiology*. 1985 Nov; 50(5):1251–1257.
- 866 **Henkel SG**, Beek AT, Steinsiek S, Stagge S, Bettenbrock K, de Mattos MJT, Sauter T, Sawodny O, Ederer M. Basic
867 Regulatory Principles of *Escherichia coli*'s Electron Transport Chain for Varying Oxygen Conditions. *PLoS ONE*.
868 2014 Sep; 9(9):e107640. doi: 10.1371/journal.pone.0107640.
- 869 **Inglede w WJ**, Poole RK. The Respiratory Chains of *Escherichia coli*. *Microbiological Reviews*. 1984; 48(3):222–271.
870 doi: 10.1128/MMBR.48.3.222-271.1984.
- 871 **Ireland WT**, Beeler SM, Flores-Bautista E, Belliveau NM, Sweredoski MJ, Moradian A, Kinney JB, Phillips R.
872 Deciphering the Regulatory Genome of *Escherichia coli*, One Hundred Promoters at a Time. *bioRxiv*. 2020 Jan;
873 doi: 10.1101/2020.01.18.910323.
- 874 **Jacob F**, Monod J. Genetic Regulatory Mechanisms in the Synthesis of Proteins. *Journal of Molecular Biology*.
875 1961 Jun; 3(3):318–356. doi: 10.1016/S0022-2836(61)80072-7.
- 876 **Jensen RB**, Wang SC, Shapiro L. A moving DNA replication factory in *Caulobacter crescentus*. *The EMBO journal*.
877 2001 Sep; 20(17):4952–4963.
- 878 **Jun S**, Si F, Pugatch R, Scott M. Fundamental Principles in Bacterial Physiology - History, Recent Progress, and
879 the Future with Focus on Cell Size Control: A Review. *Reports on Progress in Physics*. 2018 May; 81(5):056601.
880 doi: 10.1088/1361-6633/aaa628.
- 881 **Kapanidis AN**, Margeat E, Laurence TA, Doose S, Ho SO, Mukhopadhyay J, Kortkhonjia E, Mekler V, Ebright RH,
882 Weiss S. Retention of Transcription Initiation Factor Σ 70 in Transcription Elongation: Single-Molecule Analysis.
883 *Molecular Cell*. 2005 Nov; 20(3):347–356. doi: 10.1016/j.molcel.2005.10.012.

- 884 **Khademi S**, O'Connell J, Remis J, Robles-Colmenares Y, Miercke LJW, Stroud RM. Mechanism of Ammonia
885 Transport by Amt/MEP/Rh: Structure of AmtB at 1.35 Å. *Science*. 2004 Sep; 305(5690):1587–1594. doi:
886 [10.1126/science.1101952](https://doi.org/10.1126/science.1101952).
- 887 **Khademian M**, Imlay JA. *Escherichia coli* Cytochrome c Peroxidase Is a Respiratory Oxidase That Enables the
888 Use of Hydrogen Peroxide as a Terminal Electron Acceptor. *Proceedings of the National Academy of Sciences*.
889 2017 Aug; 114(33):E6922–E6931. doi: [10.1073/pnas.1701587114](https://doi.org/10.1073/pnas.1701587114).
- 890 **Li GW**, Burkhardt D, Gross C, Weissman JS. Quantifying Absolute Protein Synthesis Rates Reveals Principles
891 Underlying Allocation of Cellular Resources. *Cell*. 2014 Apr; 157(3):624–635. doi: [10.1016/j.cell.2014.02.033](https://doi.org/10.1016/j.cell.2014.02.033).
- 892 **Liu M**, Durfee T, Cabrera JE, Zhao K, Jin DJ, Blattner FR. Global Transcriptional Programs Reveal a Carbon Source
893 Foraging Strategy by *Escherichia coli*. *Journal of Biological Chemistry*. 2005 Apr; 280(16):15921–15927. doi:
894 [10.1074/jbc.M414050200](https://doi.org/10.1074/jbc.M414050200).
- 895 **Lu D**, Grayson P, Schulten K. Glycerol Conductance and Physical Asymmetry of the *Escherichia coli* Glycerol
896 Facilitator GlpF. *Biophysical Journal*. 2003 Nov; 85(5):2977–2987. doi: [10.1016/S0006-3495\(03\)74718-3](https://doi.org/10.1016/S0006-3495(03)74718-3).
- 897 **Lynch M**, Marinov GK. The Bioenergetic Costs of a Gene. *Proceedings of the National Academy of Sciences*.
898 2015 Dec; 112(51):15690–15695. doi: [10.1073/pnas.1514974112](https://doi.org/10.1073/pnas.1514974112).
- 899 **MaaløeO**. Regulation of the Protein-Synthesizing Machinery—Ribosomes, tRNA, Factors, and So On. Goldberger
900 R, editor, *Gene Expression*, Springer; 1979.
- 901 **Milo R**, Jorgensen P, Moran U, Weber G, Springer M. BioNumbers—the Database of Key Numbers in Molecular
902 and Cell Biology. *Nucleic Acids Research*. 2010 Jan; 38(suppl_1):D750–D753. doi: [10.1093/nar/gkp889](https://doi.org/10.1093/nar/gkp889).
- 903 **Monod J**. The Phenomenon of Enzymatic Adaptation and Its Bearings on Problems of Genetics and Cellular
904 Differentiation. *Growth Symposium*. 1947; 9:223–289.
- 905 **Mooney RA**, Darst SA, Landick R. Sigma and RNA Polymerase: An On-Again, Off-Again Relationship? *Molecular
906 Cell*. 2005 Nov; 20(3):335–345. doi: [10.1016/j.molcel.2005.10.015](https://doi.org/10.1016/j.molcel.2005.10.015).
- 907 **Mooney RA**, Landick R. Tethering Σ70 to RNA Polymerase Reveals High in Vivo Activity of σ Factors and Σ70-
908 Dependent Pausing at Promoter-Distal Locations. *Genes & Development*. 2003 Nov; 17(22):2839–2851. doi:
909 [10.1101/gad.1142203](https://doi.org/10.1101/gad.1142203).
- 910 **Neidhardt FC**, Ingraham JL, Schaechter M. *Physiology of the Bacterial Cell - A Molecular Approach*, vol. 1.
911 Elsevier; 1991.
- 912 **Ojkic N**, Serbanescu D, Banerjee S. Surface-to-volume scaling and aspect ratio preservation in rod-shaped
913 bacteria. *eLife*. 2019 Aug; 8:642.
- 914 **Patrick M**, Dennis PP, Ehrenberg M, Bremer H. Free RNA Polymerase in *Escherichia coli*. *Biochimie*. 2015 Dec;
915 119:80–91. doi: [10.1016/j.biochi.2015.10.015](https://doi.org/10.1016/j.biochi.2015.10.015).
- 916 **Peebo K**, Valgepea K, Maser A, Nahku R, Adamberg K, Vilu R. Proteome Reallocation in *Escherichia coli* with
917 Increasing Specific Growth Rate. *Molecular BioSystems*. 2015; 11(4):1184–1193. doi: [10.1039/C4MB00721B](https://doi.org/10.1039/C4MB00721B).
- 918 **Perdue SA**, Roberts JW. σ⁷⁰-Dependent Transcription Pausing in *Escherichia coli*. *Journal of Molecular Biology*.
919 2011 Oct; 412(5):782–792. doi: [10.1016/j.jmb.2011.02.011](https://doi.org/10.1016/j.jmb.2011.02.011).
- 920 **Phillips R**. Membranes by the Numbers. In: *Physics of Biological Membranes* Cham: Springer, Cham; 2018.p.
921 73–105.
- 922 **Ramos S**, Kaback HR. The Relation between the Electrochemical Proton Gradient and Active Transport in
923 *Escherichia coli* Membrane Vesicles. *Biochemistry*. 1977 Mar; 16(5):854–859. doi: [10.1021/bi00624a007](https://doi.org/10.1021/bi00624a007).
- 924 **Rosenberg H**, Gerdes RG, Chegwidden K. Two Systems for the Uptake of Phosphate in *Escherichia coli*. *Journal
925 of Bacteriology*. 1977 Aug; 131(2):505–511.
- 926 **Rudd SG**, Valerie NCK, Helleday T. Pathways Controlling dNTP Pools to Maintain Genome Stability. *DNA Repair*.
927 2016 Aug; 44:193–204. doi: [10.1016/j.dnarep.2016.05.032](https://doi.org/10.1016/j.dnarep.2016.05.032).
- 928 **Sánchez-Romero MA**, Molina F, Jiménez-Sánchez A. Organization of Ribonucleoside Diphosphate Reductase
929 during Multifork Chromosome Replication in *Escherichia coli*. *Microbiology*. 2011 Aug; 157(8):2220–2225. doi:
930 [10.1099/mic.0.049478-0](https://doi.org/10.1099/mic.0.049478-0).

- 931 **Schaechter M**, Maaløe O, Kjeldgaard NO. Dependency on Medium and Temperature of Cell Size and Chemical
932 Composition during Balanced Growth of *Salmonella typhimurium*. *Microbiology*. 1958 Dec; 19(3):592–606.
- 933 **Schmidt A**, Kochanowski K, Vedelaar S, Ahrné E, Volkmer B, Callipo L, Knoops K, Bauer M, Aebersold R, Heine-
934 mann M. The Quantitative and Condition-Dependent *Escherichia coli* Proteome. *Nature Biotechnology*. 2016
935 Jan; 34(1):104–110. doi: [10.1038/nbt.3418](https://doi.org/10.1038/nbt.3418).
- 936 **Scholz SA**, Diao R, Wolfe MB, Fivenson EM, Lin XN, Freddolino PL. High-Resolution Mapping of the *Escherichia*
937 *coli* Chromosome Reveals Positions of High and Low Transcription. *Cell Systems*. 2019 Mar; 8(3):212–225.e9.
- 938 **Scott M**, Gunderson CW, Mateescu EM, Zhang Z, Hwa T. Interdependence of cell growth and gene expression:
939 origins and consequences. *Science*. 2010 Nov; 330(6007):1099–1102.
- 940 **Sekowska A**, Kung HF, Danchin A. Sulfur Metabolism in *Escherichia coli* and Related Bacteria: Facts and Fiction.
941 *Journal of Molecular Microbiology and Biotechnology*. 2000; 2(2):34.
- 942 **Shi H**, Bratton BP, Gitai Z, Huang KC. How to Build a Bacterial Cell: MreB as the Foreman of E. Coli Construction.
943 *Cell*. 2018 Mar; 172(6):1294–1305. doi: [10.1016/j.cell.2018.02.050](https://doi.org/10.1016/j.cell.2018.02.050).
- 944 **Si F**, Le Treut G, Sauls JT, Vadia S, Levin PA, Jun S. Mechanistic Origin of Cell-Size Control and Homeostasis in
945 Bacteria. *Current Biology*. 2019 Jun; 29(11):1760–1770.e7. doi: [10.1016/j.cub.2019.04.062](https://doi.org/10.1016/j.cub.2019.04.062).
- 946 **Si F**, Li D, Cox SE, Sauls JT, Azizi O, Sou C, Schwartz AB, Erickstad MJ, Jun Y, Li X, Jun S. Invariance of Initiation Mass
947 and Predictability of Cell Size in *Escherichia coli*. *Current Biology*. 2017 May; 27(9):1278–1287.
- 948 **Sirko A**, Zatyka M, Sadowy E, Hulanicka D. Sulfate and Thiosulfate Transport in *Escherichia coli* K-12: Evidence
949 for a Functional Overlapping of Sulfate- and Thiosulfate-Binding Proteins. *Journal of Bacteriology*. 1995 Jul;
950 177(14):4134–4136. doi: [10.1128/jb.177.14.4134-4136.1995](https://doi.org/10.1128/jb.177.14.4134-4136.1995).
- 951 **Stasi R**, Neves HI, Spira B. Phosphate Uptake by the Phosphonate Transport System PhnCDE. *BMC Microbiology*.
952 2019 Apr; 19. doi: [10.1186/s12866-019-1445-3](https://doi.org/10.1186/s12866-019-1445-3).
- 953 **Stevenson BS**, Schmidt TM. Life History Implications of rRNA Gene Copy Number in *Escherichia coli*. *Applied*
954 and Environmental Microbiology. 2004 Nov; 70(11):6670–6677. doi: [10.1128/AEM.70.11.6670-6677.2004](https://doi.org/10.1128/AEM.70.11.6670-6677.2004).
- 955 **Stouthamer AH**. A Theoretical Study on the Amount of ATP Required for Synthesis of Microbial Cell Material.
956 *Antonie van Leeuwenhoek*. 1973 Dec; 39(1):545–565. doi: [10.1007/BF02578899](https://doi.org/10.1007/BF02578899).
- 957 **Stouthamer AH**, Bettenhaussen CW. A continuous culture study of an ATPase-negative mutant of *Escherichia*
958 *coli*. *Archives of Microbiology*. 1977 Jun; 113(3):185–189.
- 959 **Svenningsen SL**, Kongstad M, Stenum TS, Muñoz-Gómez AJ, Sørensen MA. Transfer RNA Is Highly Unstable
960 during Early Amino Acid Starvation in *Escherichia coli*. *Nucleic Acids Research*. 2017 Jan; 45(2):793–804. doi:
961 [10.1093/nar/gkw1169](https://doi.org/10.1093/nar/gkw1169).
- 962 **Szenk M**, Dill KA, de Graff AMR. Why Do Fast-Growing Bacteria Enter Overflow Metabolism? Testing the
963 Membrane Real Estate Hypothesis. *Cell Systems*. 2017 Aug; 5(2):95–104. doi: [10.1016/j.cels.2017.06.005](https://doi.org/10.1016/j.cels.2017.06.005).
- 964 **Taheri-Araghi S**, Bradde S, Sauls JT, Hill NS, Levin PA, Paulsson J, Vergassola M, Jun S. Cell-size control and
965 homeostasis in bacteria. - PubMed - NCBI. *Current Biology*. 2015 Feb; 25(3):385–391.
- 966 **Tatusov RL**, Galperin MY, Natale DA, Koonin EV. The COG database: a tool for genome-scale analysis of protein
967 functions and evolution. *Nucleic Acids Research*. 2000 Jan; 28(1):33–36.
- 968 **Taymaz-Nikerel H**, Borujeni AE, Verheijen PJT, Heijnen JJ, van Gulik WM. Genome-Derived Minimal
969 Metabolic Models for *Escherichia coli* MG1655 with Estimated in Vivo Respiratory ATP Stoichiometry.
970 *Biotechnology and Bioengineering*. 2010; 107(2):369–381. doi: [10.1002/bit.22802](https://doi.org/10.1002/bit.22802), _eprint:
971 <https://onlinelibrary.wiley.com/doi/pdf/10.1002/bit.22802>.
- 972 **The Gene Ontology Consortium**. The Gene Ontology Resource: 20 years and still GOing strong. *Nucleic Acids*
973 *Research*. 2018 Nov; 47(D1):D330–D338.
- 974 **Valgepea K**, Adamberg K, Seiman A, Vilu R. *Escherichia coli* Achieves Faster Growth by Increasing Catalytic and
975 Translation Rates of Proteins. *Molecular BioSystems*. 2013; 9(9):2344. doi: [10.1039/c3mb70119k](https://doi.org/10.1039/c3mb70119k).
- 976 **Weber J**, Senior AE. ATP Synthesis Driven by Proton Transport in F1FO-ATP Synthase. *FEBS Letters*. 2003;
977 545(1):61–70. doi: [10.1016/S0014-5793\(03\)00394-6](https://doi.org/10.1016/S0014-5793(03)00394-6).

- 978 **Willsky GR**, Bennett RL, Malamy MH. Inorganic Phosphate Transport in *Escherichia coli*: Involvement of Two
979 Genes Which Play a Role in Alkaline Phosphatase Regulation. *Journal of Bacteriology*. 1973 Feb; 113(2):529–
980 539.
- 981 **Zhang L**, Jiang W, Nan J, Almqvist J, Huang Y. The *Escherichia coli* CysZ Is a pH Dependent Sulfate Transporter That
982 Can Be Inhibited by Sulfite. *Biochimica et Biophysica Acta (BBA) - Biomembranes*. 2014 Jul; 1838(7):1809–1816.
983 doi: [10.1016/j.bbamem.2014.03.003](https://doi.org/10.1016/j.bbamem.2014.03.003).
- 984 **Zhang Z**, Aboulwafa M, Saier MH. Regulation of Crp Gene Expression by the Catabolite Repressor/Activator,
985 Cra, in *Escherichia coli*. *Journal of Molecular Microbiology and Biotechnology*. 2014; 24(3):135–141. doi:
986 10.1159/000362722.
- 987 **Zhu M**, Dai X. Growth suppression by altered (p)ppGpp levels results from non-optimal resource allocation in
988 *Escherichia coli*. *Nucleic Acids Research*. 2019 Mar; 47(9):4684–4693.